FABRICATION AND EVALUATION OF SULFONATED POLY(ETHER ETHER KETONE) AND FLUORIDATED HYDROXYAPATITE COMPOSITE SCAFFOLDS FOR BONE TISSUE ENGINEERING

A THESIS SUBMITTED TO
THE GRADUATE SCHOOL OF NATURAL AND APPLIED SCIENCES
OF
MIDDLE EAST TECHNICAL UNIVERSITY

BY

ATAOLLAH NOSRATINIA

IN PARTIAL FULFILLMENT OF THE REQUIREMENTS
FOR
THE DEGREE OF MASTER OF SCIENCE
IN
BIOTECHNOLOGY

May 2022

Approval of the thesis:

FABRICATION AND EVALUATION OF SULFONATED POLY(ETHER ETHER KETONE) AND FLUORIDATED HYDROXYAPATITE COMPOSITE SCAFFOLDS FOR BONE TISSUE ENGINEERING

submitted by **ATAOLLAH NOSRATINIA** in partial fulfillment of the requirements for the degree of **Master of Science in Biotechnology, Middle East Technical University** by,

Prof. Dr. Halil Kalıpçılar
Dean, Graduate School of **Natural and Applied Sciences** _____

Assoc. Prof. Yeşim Soyer
Head of the Department, **Biotechnology** _____

Prof. Dr. Dilek Keskin
Supervisor, **Biotechnology, METU** _____

Prof. Dr. Zafer Evis
Co-Supervisor, **Engineering Sciences, METU** _____

Examining Committee Members:

Prof. Dr. Caner Durucan
Metallurgical and Materials Eng, METU _____

Prof. Dr. Dilek Keskin
Engineering Sciences, METU _____

Prof. Dr. Ayşen Tezcaner
Engineering Sciences, METU _____

Prof. Dr. Sreeparna Banerjee
Biological Sciences, METU _____

Assist. Prof. Dr. Ali Deniz Dalgıç
Genetics and Bioengineering, Istanbul Bilgi University _____

Date: 27.05.2022

I hereby declare that all information in this document has been obtained and presented in accordance with academic rules and ethical conduct. I also declare that, as required by these rules and conduct, I have fully cited and referenced all material and results that are not original to this work.

Name Last name : Ataollah Nosratinia

Signature :

ABSTRACT

FABRICATION AND EVALUATION OF SULFONATED POLY(ETHER ETHER KETONE) AND FLUORIDATED HYDROXYAPATITE COMPOSITE SCAFFOLDS FOR BONE TISSUE ENGINEERING

Nosratinia, Ataollah
Master of Science, Biotechnology
Supervisor : Prof. Dr. Dilek Keskin
Co-Supervisor: Prof. Dr. Zafer Evis

May 2022, 60 pages

Poly (ether ether ketone) (PEEK) has attracted the interest of bone tissue engineers due to its close range of mechanical properties to that of human bones, its biocompatibility, and excellent chemical resistance. However, PEEK is bioinert and has very low hydrophilicity. Sulfonation can compensate for this by introducing hydrophilic sulfonate groups. Furthermore, hydroxyapatite (HA) which is the main component of the bone, can introduce bioactivity to the scaffold. Compared to pure HA, Fluoridated hydroxyapatite (FHA) has higher stability and possesses higher osteogenic activity. In this context, FHA was prepared and combined with previously prepared Sulfonated PEEK (sPEEK). Wet-electrospinning method was used to make sPEEK scaffolds combined with HA and FHA in 1%, 2.5%, and 5% ratios for bone tissue engineering. SEM Analysis, FTIR Analysis, Mechanical Strength tests, Water uptake measurement, *in vitro* degradation assay, Simulated Body Fluid assay, and cell attachment and proliferation assay were performed. Even though toxic at high concentrations, HA and FHA at ratios that were combined with sPEEK to form electrospun scaffolds showed good cell viability and improved proliferation at the optimum concentrations. Scaffolds show mineralization in the SBF solution and tend to gradually degrade in PBS. In vitro experiments with Saos-2 cells show that FHA in optimum ratios is less cytotoxic than HA and incorporation of both HA and FHA in

optimum ratios into the sPEEK scaffolds enhance cell proliferation. Among groups, considering all properties 1% FHA*sPEEK can be suggested as the most promising one. It is concluded that the scaffolds are cytocompatible and provide a desirable environment for cell growth and proliferation.

Keywords: Bone tissue engineering, sPEEK, Fluorohydroxyapatite, Electrospinning

ÖZ

KEMİK DOKU MÜHENDİSLİĞİ İÇİN SÜLFONATLI POLİ(ETER ETER KETON) VE FLORÜRLÜ HİDROKSİAPATİT KOMPOZİT İSKELELERİN İMALATI VE DEĞERLENDİRİLMESİ

Nosratinia, Ataollah
Yüksek Lisans, Biyoteknoloji
Tez Yöneticisi: Prof. Dr. Dilek Keskin
Ortak Tez Yöneticisi: Prof. Dr. Zafer Evis

Mayıs 2022, 60 sayfa

Poli (eter eter keton) (PEEK), insan kemiklerine yakın mekanik özellikleri, biyouyumluluğu ve mükemmel kimyasal direnci nedeniyle kemik dokusu mühendislerinin ilgisini çekmiştir. Bununla birlikte, PEEK biyoinerttir ve çok düşük hidrofilikliğe sahiptir. Sülfonasyon, hidrofilikliğe ekleyerek ve biyoaktif sülfonat grupları ekleyerek bunu telafi edebilir. Ayrıca kemiğin ana bileşeni olan hidroksiapatit (HA) iskeleye biyoaktivite katabilir. Saf HA ile karşılaştırıldığında, Florlu hidroksiapatit (FHA) daha yüksek stabiliteye sahiptir ve daha yüksek osteojenik aktiviteye sahiptir; hazırlandp onceden hazırlanan Sulfone PEEK (sPEEK) ile birleştirilde. Kemik doku mühendisliği için HA ve FHA ile birlikte %1, %2,5 ve %5 oranlarında sPEEK yapı iskeleleri yapmak için wet-elektrospinning yöntemi kullanılmıştır. Ardından SEM Analizi, FTIR Analizi, Mekanik Mukavemet testleri, Su alımı ölçümü, *in vitro* degradasyon testi, Simüle Vücut Sıvısı testi, hücre tutunma ve çoğalma testi yapılmıştır. Yüksek konsantrasyonlarda toksik olmasına rağmen, elektrospun yapı iskeleleri oluşturmak için sPEEK ile birleştirilen oranlarda HA ve FHA, hücre canlılığı göstermiş ve optimum konsantrasyonlarda proliferasyonu artırdığı görülmektedir. İskeleler, SBF çözeltisinde mineralizasyon gösterir ve PBS'de kademeli olarak bozulma eğilimindedir. Saos-2 hücreleriyle yapılan in vitro deneyler, optimum oranlarda FHA'nın HA'dan daha az sitotoksik olduğunu ve hem HA hem de

FHA'nın optimum oranlarda sPEEK yapı iskelelerine dahil edilmesinin hücre çoğalmasını arttırdığını göstermektedir. Gruplar arasında tüm özellikler göz önüne alındığında %1 FHA*sPEEK en umut verici olanı olarak önerilebilir. İskelelerin sito-uyumlu olduğu ve hücre büyümesi ve çoğalması için uygun bir ortam sağladığı sonucuna varılmıştır.

Anahtar Kelimeler: Kemik dokusu mühendisliği, sPEEK, Florlu hidroksiapatit, Elektroeğirme

To my dearest family for incredible love and everlasting support…

ACKNOWLEDGMENTS

I wish to express my deepest gratitude to my supervisor Prof. Dr. Dilek Keskin and co-advisor Prof. Dr. Zafer Evis for their insightful guidance and advice throughout my research.

I wish to express similar gratitude to Assist. Prof. Ali Deniz Dalgıç who was a senior research assistant in the Biomaterial Laboratory at the time, for introducing me to the laboratory and teaching me in addition to his friendship.

I would like to thank all my labmates for all the things they taught me and for their sincere, welcoming, and helpful attitudes.

I want to thank all my friends for the great discussions and fun times we had together.

This work is funded by the Middle East Technical University Scientific Research Projects Coordination Unit under the BAP project with the 10878 ID number.

TABLE OF CONTENTS

LIST OF TABLES

TABLES

LIST OF FIGURES

FIGURES

LIST OF ABBREVIATIONS

ABBREVIATIONS	
ALP	: Alkaline Phosphatase
CaP	: Calcium Phosphate
COL I	: Collagen Type I
DMEM	: Dulbecco's Modified Eagle Medium
DMSO	: Dimethyl Sulfoxide
DMAc	: Dimethyl Acetamide
EDX	: Energy Dispersed X-Ray
EtOH	: Ethyl Alcohol
FBS	: Fetal Bovine Serum
FHA	: Fluorohydroxyapatite
FTIR	: Fourier-Transform Infrared Spectroscopy
HA	: Hydroxyapatite
MSCs	: Mesenchymal Stem Cells
MTT	: (3-(4,5-Dimethylthiazol-2-Yl)-2,5-Diphenyltetrazolium Bromide)
OC	: Osteocalcin
PBS	: Phosphate Buffer Saline
PCL	: Poly(Caprolactone)
PDLLA	: Poly(L-Lactide-Co-D,L-Lactide)
PEEK	: Polyether Ether Ketone
PFA	: Paraformaldehyde

SEM : Scanning Electron Microscopy

sPEEK : Sulfonated Polyether Ether Ketone

TGF-β : Transforming Growth Factor B

XRD : X-Ray Diffraction Analysis

CHAPTER 1

INTRODUCTION

1.1 Structure of the Bone and Related Disorders

1.1.1 Structure of the Bone

Bone is the hard tissue in the human skeletal system. This property enables it to perform its roles as support and protection of other tissues and organs while it performs other roles such as depositing minerals and participation in keeping the blood hemostasis. It is mainly constituted of Hydroxyapatite (HA) (up to 50%v,70%w)(Zhang & Rehmmann, 2022) in combination with organic components (like proteins) and water. High strength to weight ratio and functional proficiency of the bone is the result of its fine-tuned architecture composing of two main forms. The dense and rigid form (about 80% of the whole skeleton) is called cortical bone, and the spongy form known as cancellous or trabecular bone (about 20% of the total skeleton)(B, 2008). The whole surface of the bone except where is covered by cartilage and the attaching points of tendons and ligaments is covered by a membrane called the periosteum which has a critical part in bone regeneration in mineralization, vascularization, and protection(Xin et al., 2017). Cortical bone has an intricate hierarchical order from nano to macro scale which takes the name "Haversian system"(Clarke, 2008). The Haversian system is made up of Osteons which are canals with mineral matrix containing neurons, blood vessels, and lymph. An osteon consists of a central osteonic/Haversian canal surrounded by distinct concentric rings of matrix called Lamellae which are made due to changing orientation of collagen fibers in each layer perpendicular to the other layers which provides obvious advantages in baring especially tensile stress(*Cartilage, Bone & Ossification: The Histology Guide*, n.d.). Cells are in spaces between layers called lacunae. Cells and lacunae are connected by microscopic canals called canaliculi. The spongy bone, on the other hand, consists of

interconnected thin and narrow bone, forming bars and plate-shaped borders for cavities called trabeculae. The trabeculae are arranged and can realign in the direction of stress. The canaliculi in spongy bone are connected to the nearby cavity in comparison to the ones in the compact bone that are rooted at the central osteonic canal for the blood supply(*Cartilage, Bone & Ossification: The Histology Guide*, n.d.). Compact bone provides resistance to tension, compression, and torsion, whereas the porous bone structure is primarily beneficial for reducing the weight of the bone, and it houses the bone marrow(Cooke et al., 2016). Table 1 shows mechanical properties of natural bone.

Table 1. Natural bone mechanical properties(Tereshchenko et al., 2015)

	Compact bone	Cancellous bone
Tensile Strength (MPa)	50-150	10-100
Compressive strength (MPa)	130-230	2-12
Young's modulus (GPa)	7-30	0,02-0,5
Stretching before break (%)	1-3	5-7
Shear modulus (GPa)	3	3

Bones in human body are classified into 5 types differing in anatomical shape namely: Long, short, flat, sesamoid, and irregular bones.

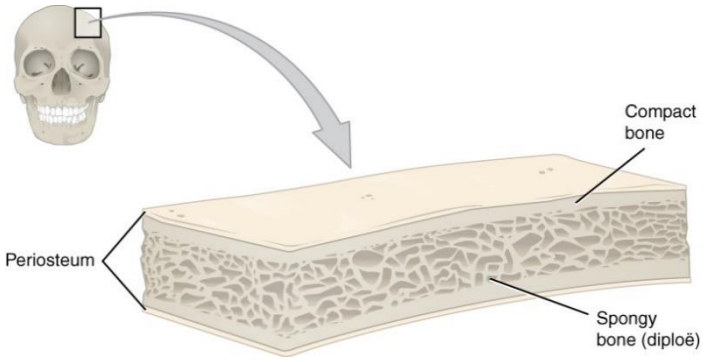

Figure 1. Flat bone anatomy(Dong et al., 2021)

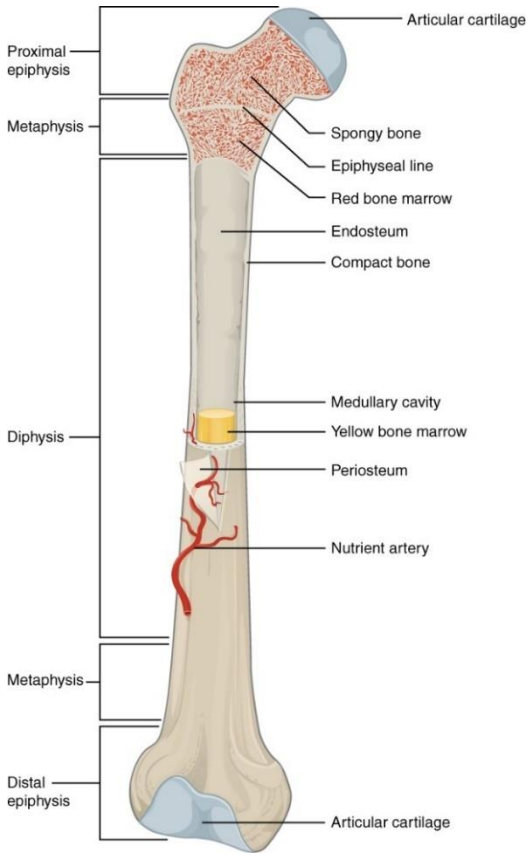

Figure 2. Long bone anatomy(*Bone Structure – Anatomy & Physiology*, n.d.)

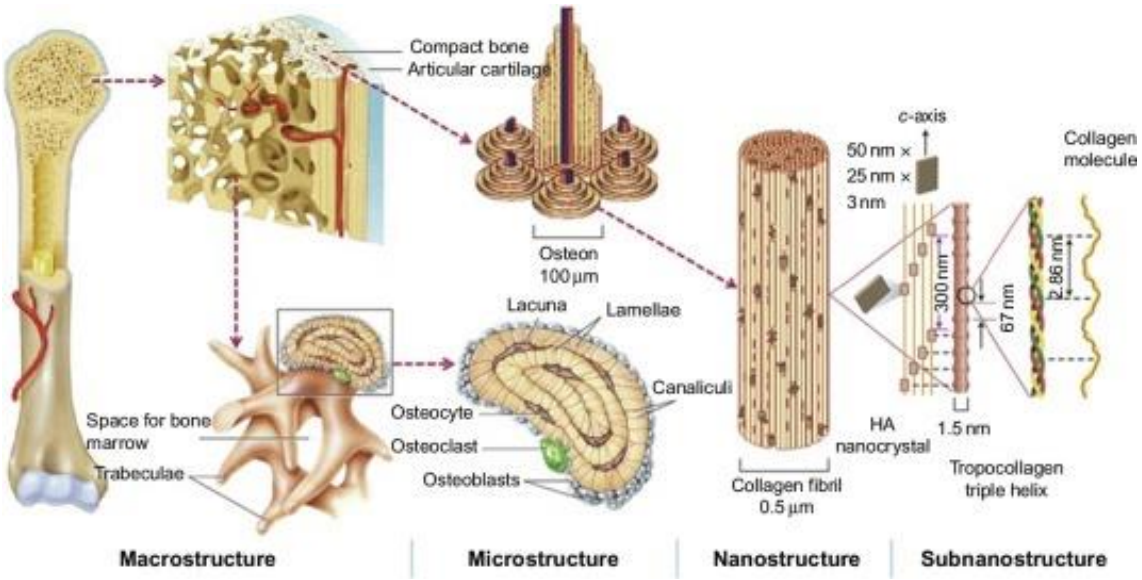

Figure 3. Bone structure(McGee-Lawrence et al., 2013)

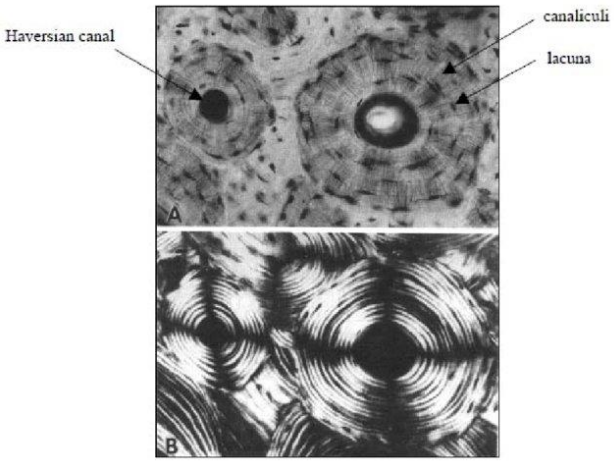

Figure 4.(A) A histological cross section of cortical bone showing the Osteons (B) Same cross-section in polarized light showing osteon's numerous concentric lamellae (Verbruggen, 2013)

Bone marrow

Bone marrow is the organ that exists in most mammals and is the primary center of hematopoiesis which is the mechanism that blood cells are produced from Hematopoietic stem cells, a certain class of multipotent stem cells in adults. Bone marrow is dividable into two main types, yellow bone marrow (Mesenchymal Stem Cells) primarily in the medullary cavity in the diaphysis of long bones and red bone marrow (Hematopoietic Stem Cells) primarily in flat bones (McGee-Lawrence et al., 2013).

1.1.2 Cells present in Bone Tissue

Bone tissue consists of hard extracellular matrix and cellular constituent (about up to 5%)(*Bone - Chemical Composition and Physical Properties | Britannica*, n.d.). The natural plasticity of skeletal system is due to two main phases in the bone remodeling mechanism, namely: bone resorption and bone formation (Figure 5). Osteoblast cells drive the bone formation and osteoclasts are the main cell type responsible for bone

resorption, whilst Osteocytes regulate the process (Delaisse, 2014). These cells along with the bone lining cells, make up the four main cell types of the osseous tissue.

Bone homeostasis is kept by constant remodeling which consists of activation, resorption, reversal, formation, and mineralization before and after resting phases.(Truesdell et al., 2020) Remodeling begins with osteocytes responding to physical or metabolic signals such as microcracks or hormone signals. An example of this is when osteocytes go through apoptosis under physiologic or metabolic stress. At the resting state transforming growth factor β (TGF-β) is secreted from the bone osteocytes inhibiting the osteoclastogenesis; osteocyte apoptosis results in decline of TGF-β levels, triggering the osteoclastogenesis(Raggatt & Partridge, 2010).

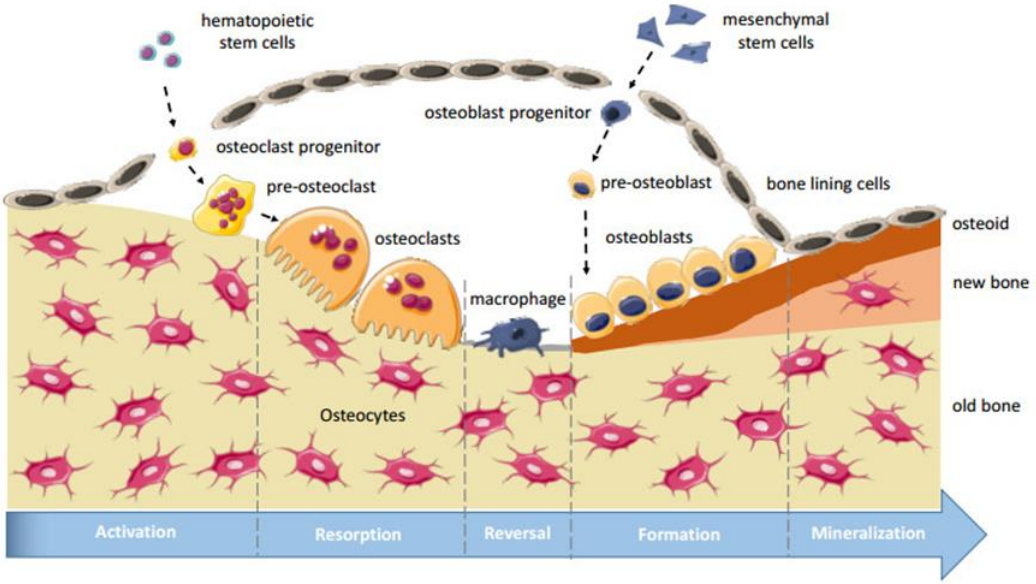

Figure 5. Schematic representation of bone remodeling process(Truesdell et al., 2020)

The most abundant (90% to 95%) cell type present in the osseus tissue are the Osteocytes(Schaffler & Kennedy, 2012). Osteocytes are interconnected stellate(Rutkovskiy et al., 2016) cells driven from osteoblast cell line and have crucial regulatory functions such as triggering the onset of bone formation and resorption, regulation of mineral deposition in bone matrix and effecting other organs like kidneys (bone-kidney axis) by releasing endocrine factors to regulate systemic phosphate

transport. Also, osteocytes regulate osteoclasts and osteoblasts according to their sense of the mechanical load on the bone tissue in the form of deformation and fluid movement in the lacunar-canalicular spaces. In their regulation they are sensitive to endocrine factors such as metabolic and sex hormones(Schaffler & Kennedy, 2012).

Osteoblasts known as bone-forming cells, may come from two origins, the neural ectoderm which then only make up parts of the skull, or directly from condensed mesenchymal progenitors without intermediate stages, that is the source for the formation of the rest of the skeleton. Osteoblasts encircled by the bone matrix turn into osteocytes, being post-mitotic cells, the ones on the surface of the bone facing the periosteum after being derived from mesenchymal stem cells either go through apoptosis or turn into bone-lining cells. Osteoblasts have a cuboidal shape and perform a central role in all three bone formation processes namely osteogenesis, modeling, and remodeling. Osteoblasts secrete the bone matrix and the matrix proteins including type I collagen (COL I), alkaline phosphatase (ALP) and osteocalcin (OC)(Rutkovskiy et al., 2016).

Bone lining cells are the inactive osteoblasts that are in the surface of the bone in the contrast with osteocytes that are inside the extracellular bone matrix. They are long, slender, and flat and have the potential to become active osteoblasts.

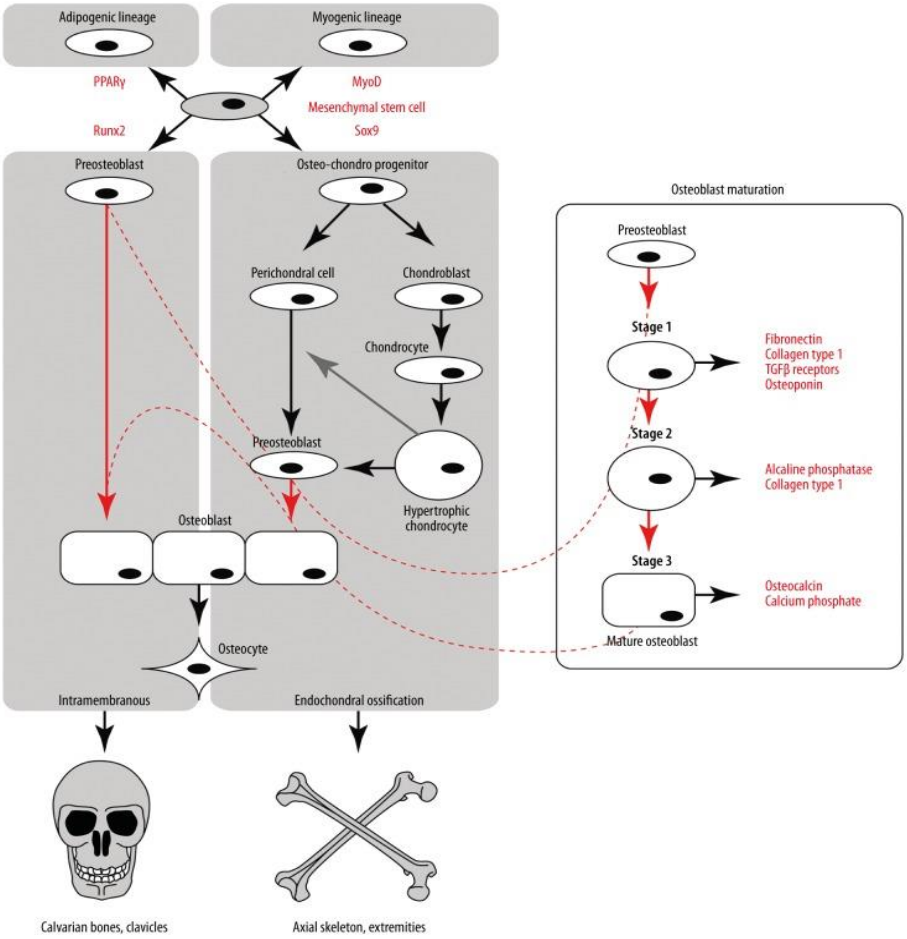

Figure 6. Lineage and differentiation flowchart of osteoblasts and osteocytes(Rutkovskiy et al., 2016)

Osteoclasts resorb the bone by secreting proteases and hydrochloric acid (HCL) into a lysosomal compartment at their basal cell membrane. In many pathologic conditions the amount of bone resorbed by osteoclasts exceeds the amount of regenerated bone by osteocytes. The origin of osteoclasts is circulating monocytes derived from myeloid lineage. They get attracted to the sides of bone marked for resorption and make multinucleated cells on the surface. Osteoblasts have a predominant effect on the formation of osteoclast by releasing cytokines(Boyce et al., 2009).

1.1.3 Bone Matrix

Bone mainly comprises of cells and extracellular matrix. The ECM of the bone is dividable to organic and inorganic (mineral) phases. Bone by the net weight account, is comprised of 60% inorganic material, 25% organic material and 5% water. By volume, bone is 36% inorganic, 36% organic and 28% water.

The inorganic/mineral phase composes of calcium and phosphate formed into needle-like or thin plates of HA crystals. The crystals have very small substitution of magnesium carbonate, sodium, potassium, fluorine, chloride, and other ions present in physiological fluids. The organic matrix is mainly composed of collagen (about 90%) which is mainly type I collagen secreted by osteoblasts. Other organic materials are mainly endogenous to the osseus tissue, but some are originated in different parts of the body and then transported by the circulatory system(Mohamed, 2008).

1.1.4 Hydroxyapatite

Bone apatite is mostly referred to as HA since it is a nanocrystal of carbonated, basic calcium phosphate arranged in apatite form. Toughness and pressure bearing ability of the bone is driven from the inorganic part that is mainly HA(Vallet-Regí & Navarrete, 2015). Many trials have been done to produce the same characteristics by the synthetic HA due to its close stoichiometric similarity to the bone apatite in the last four decades, but they have not been quite successful. Major short comings include mechanical property insufficiency, unsuitable degradation rate and insufficient biological quality like poor osteogenesis and angiogenesis induction. The reason behind this is that the naturally accruing bone apatite is in a nanoarchitecture reinforced by gelatin and other organic and inorganic compounds. Furthermore, slight structural and compositional difference are noticeable since in the natural in vivo environment ion exchanges cause formation of other ion substituted apatite, plus crystalline structure and percentage is predictably different. This can be shown clearly in respective chemical formulas whereas $[Ca_{10}(PO_4)_6(OH)_2]$ represents pure synthetic HA while the following belongs to the bone apatite $[Ca_{10}–(x–$

u)$(PO_4)_6$−x(HPO_4orCO3)x(OH,F..)(2–(x−2u))],where $0 \leq x \leq 2$, $0 \leq 2u \leq x$. To address these issues researchers have tried coping different ions with the synthetic apatite, use growth factors, use composites of different combinations along with otheras(Kulanthaivel et al., 2015).

1.1.5 Bone defects

There are hereditary or attained conditions that compromise bone tissue integrity. Developmental problems accrue in bone and cartilage which are known under the general term of Osteochondrodysplasia(Cooke et al., 2016). Other than genetic disorders tumors and autoimmune diseases can also compromise the integrity of the bone tissue.

Bone, made up of HA, is naturally brittle. Collagen netting provides relative elasticity to the tissue, but it is still susceptible to breaks and injuries. The natural plasticity compensates for this to a certain degree but in cases exceeding the critical size threshold (typically >2 cm, depending on the anatomical site)(Koons et al., 2020) full recovery exceeds body's potential to heal without interference.

1.2 Bone Tissue Engineering

Rise of life expectancy, obesity and poor physical activity are adding to the pathologic conditions in bone tissue health and the urgency of addressing them in modern world populations. Traditionally grafts (autologous, allogeneic, and xenogeneic transplants) have been used for addressing the clinical need of replacing bone tissue. Grafting bone has its own dangers and limitations. For instance, autogenous implants requirement for additional surgery and then the donor site morbidity in addition to lack of availability are serious drawbacks for their widespread use. On the other hand, allogenous and exogenous scaffolds have high risk of disease transmission and immunogenicity(Ghassemi et al., 2018). Attention has been attracted to bone tissue engineering as a potential alternative approach eliminating these dangers and

limitations(Amini et al., 2012a). Tissue engineering is a field of study to develop tissue scaffolds or regeneration approaches for maintaining, replacing or improving the function of damaged tissues by coupling engineering knowledge with life sciences(Rahmati et al., 2021).

1.2.1 Scaffolds

Bone scaffold is a three-dimensional biomaterial used for bone defect reconstruction. An ideal scaffold should fill the gap caused by defects and possess certain features such as biocompatibility meaning improving cell adhesion and proliferation without inflammation induction or toxicity, osteogenic differentiation, controlled biodegradability and integrability for safe osteoid substitution; also osteoconductivity which supports and improves cell adhesion, proliferation and migration(Van Gaalen et al., 2008). Porosity, proper pore size and interconnectivity of the pores that are critical for cell penetration and attachment, nutrients and waste transfer, and vascularization therefore, porous scaffolds enhance the regeneration of the bone tissue(Van Gaalen et al., 2008). The suitable pore sizes in diameter is defined in the range of 100-600 μm (Vaezi & Yang, 2015) to allow biomaterial vascularization. In addition to those, controlled deliverability of bioactive molecules or drugs, sterilizability without compromising the bioactivity and, if necessary, load bearing capacity(Amini et al., 2012a),(Tariverdian et al., 2019) are important. Scaffolds for bone tissue can be developed by a wide range of strategies. The techniques that have been used to produce functional scaffolds include compression molding(Wong et al., 2009), selective laser sintering (SLS)(Kim et al., 2009), Electrospinning, and gas foaming(Tariverdian et al., 2019), Self-assembly, Phase Separation, Solvent Casting, Freeze Drying, and 3D Printing(Rahmati et al., 2021).

Researchers are investigating the production of scaffolds that have high structural and functional similarity to natural tissues to compensate for the lost structure and/or function (Sefat et al., 2019). It can be for substituting the imperfection resulted from the defect, regenerate the lost tissue or both at the same time. Therefore, a temporary or permanent mechanical integrity needs to be provided for achieving these objectives,

the scaffold is the best when it has similar properties to the bone tissue. Since it should meet the demands of the surrounding tissue and provide the correct mechanotransduction for tissue repair(Amini et al., 2012b).

1.2.2 Material used in bone tissue engineering

Ceramic, polymeric, and metallic materials as well as co-polymers, polymer-polymer blends, polymer-ceramic composites, polymer/metal or metal/ceramic composite alongside the advanced hydrogels and immune-modulatory biomaterials have been used to create bone implants and scaffolds(Ghassemi et al., 2018)·(Amini et al., 2012a).

1.2.2.1 Bioceramics

Bioceramics are very similar to bone tissue since the major part of the bone is made of HA. In comparison to other materials, they can better enhance osteoblasts adherence and proliferation. Calcium phosphate ceramics (CPCs) as tunable bioactive materials have been under investigation for a long time. Because of their properties they are very osteoconductive and osteoinductive. HA, tricalcium phosphate (TCP), and combination of them as amorphous calcium phosphates (biphasic calcium phosphate) are very commonly used in bone tissue engineering. Recently it has been shown that addition of calcium phosphate can be used to modify the dissolution rate, mechanical strength, and biocompatibility of the scaffold(Ghassemi et al., 2018).

Ceramics have better mechanical strength in comparison to polymers, but still inferior to natural bones' properties especially in torsion and tensile strength. For instance, compressive (500-1000 MPa) and bending strength (115-200 MPa) of HA is higher in comparison with the human cortical bone (100-230 and 50-150 MPa respectively);

but its fracture toughness (1 MPa $m^{0.5}$) is lesser (2-12 MPa $m^{0.5}$) than bone's(Ghassemi et al., 2018).

1.2.2.1.1 FHA

Hydroxyapatite, as the main inorganic component of the bone matrix is also the most studied bioceramic for bone tissue engineering applications. However, there are limitations related to HA; for instance, by sintering HA to above 850 °C for increasing the mechanical strength, it starts to decompose into other calcium phosphate forms, causing a weakness in structure and high resorbability that in turn result in poor biocompatibility. Partial replacement of the hydroxyl group in the HA with fluorine results in fluorohydroxyapatite (FHA), which resolves the mentioned issues. Furthermore, studies on FHA suggest a better biocompatibility in comparison to HA. Also, it has been shown that FHA's thermal stability is higher than HA's which results from reduction of the decomposition into TCP. TCP shows a higher resorption rate in comparison to HA and FHA, but by controlling its amount, TCP can also be used to modify the resorption rate(Ghassemi et al., 2018).

1.2.2.2 Polymers

Polymers can be divided into natural and synthetic. Synthetic polymers are more versatile and potent for chemical modification and molecular alteration. Their suitable mechanical properties can be considered as an important factor in choosing them as a component of the scaffolds. Extensively used synthetic polymers are mostly aliphatic polyesters. They are namely: Poly(L-lactic acid) (PLLA), polylactide-co-glycolide (PLGA; a copolymer of lactic acid and glycolic acid with different copolymer contents), polycaprolactone (PCL), polypropylene fumarate (PPF), polyethylene glycol (PEG) and polyethylene oxide (PEO). Other than these, poly(methyl methacrylate), poly(e-caprolactone), polyethylene, polypropylene, polyurethane, poly(-ethylene terephthalate), Polybutylene terephthalate (PBT), poly ether ketone,

Poly glycolic acid (PGA), Polyethylene terephthalate (PET), Polyvinyl alcohol (PVA), Poly(propylene fumarate) (PPF), polyacrylic acid (PAA), and Polyurethane (PUR & PU), and poly(sulfone) are among synthetic polymers utilized for bone tissue engineering. Natural polymers are categorized in 3 main classes: 1) Proteins, 2) Polysaccharides, and 3) Polynucleotides. Common proteins that are used in bone tissue engineering are collagen, gelatin, fibrinogen, elastin, keratin, and silk while glycosaminoglycans, cellulose, amylose, dextran, and chitin are among commonly used polysaccharides. Usually, the final structure contains both natural and synthetic polymers but normally the natural polymer total composition ratio doesn't exceed 10% but already makes a great improvement in the scaffold biocompatibility and other properties in comparison to the one made of purely synthetic polymers. Natural polymers show great biocompatibility and controllable biodegradation, but they have low mechanical properties(Ghassemi et al., 2018)·(Koons et al., 2020).

It's worth highlighting that collagen type I is the main protein of bone tissue ECM. It has nano fibrillar structure that is important for cell attachment, proliferation, and differentiation. Gelatin is obtained from collagen by hydrolysis, having almost the same composition and properties. It is a denatured biopolymer and despite Collagen, avoids immunogenicity and pathogen transmission concerns. Both of them are widely studied and used natural biomaterial (X. Liu et al., 2009).

1.2.2.3 PEEK

Polyether Ether Ketone (PEEK) is a semicrystalline high-temperature structural thermoplastic from a broader class of plastics called Polyaryletherketones (PAEKs). It was first introduced in 1977 by Imperial Chemical Industries, UK. The extensive use of PEEK as a biomaterial goes back to 1980s and it has been shown to have favorable properties such as high mechanical strength (especially similar elastic modulus to bone and low friction coefficient) (Table 2.), biocompatibility, resistance to chemical damage, radiolucency, and antimicrobial effects of its surface against some bacterial species. Since PEEK is only dissolvable in sulfuric acid and not very

chemically functional at its base form, it is usually functionalized by sulfonation(Zhao et al., 2019),(Brum et al., 2019),(Pimentel et al., 2019),(Alam et al., 2020).

Table 2. Properties of PEEK(*Polyetheretherketone (PEEK) - Polyetherether Ketone (PEEK) - Matmatch*, n.d.)

Property	**Value**
Dielectric Constant (at 20°C)	2.8 - 3.2
Dielectric Strength (kV/mm)	190 at 23 °C
Elongation at Break (%)	15 - 50
Impact Strength (kJ/m²)	4 - 10 at 20 °C
Elastic Modulus (GPa)	3.5 – 4.1
Maximum allowed stress (MPa)	90 - 120
Coefficient of thermal expansion (1/K)	4.5E-5 - 6E-5
Density (g/cm^3)	1.3 - 1.35
Thermal conductivity (W/m.K)	0.25 – 0.29
Melting point (°C)	340 - 345
Specific heat capacity (J/(kg·K))	2100 - 2200 at 20 °C

1.2.3 Electrospinning

Electrospinning has increasing attracted researchers' attention since the late 20th century. Several types of electrospinning have been developed that could be performed in vertical or horizontal set up, which are namely: Basic Needle Based Electrospinning, Multi-axial Electrospinning (coaxial or tri-axial), Bi-component Electrospinning, Multi-needle Electrospinning, Electroblowing/Gas-assisted/Gas jet Electrospinning, Magnetic Field Assisted Electrospinning, Conjugate

Electrospinning, Centrifugal Electrospinning, Needleless Electrospinning(Haider et al., 2018).

In basic needle-based electrospinning, the electrostatic force draws the fibers produced from a charged polymer solution at the tip of a syringe onto a collector connected to ground. This happens when the electric repulsion caused by charge accumulation in the droplet (at the tip of the spinneret) overcomes the surface tension of the liquid, this is followed by a thread of the solution streaming towards the collector (if the solution has high enough molecular cohesion, otherwise it will be sprayed). The collector can be a bath of liquid which the polymer doesn't dissolve in (wet spinning) or a solid plate in either horizontal or vertical position (dry spinning). The point that the stream erupts from the droplet is called the Taylor cone. The stream dries up while flying towards the collector and usually there is a controlled air flow to facilitate this transition. As the stream dries, the transition from liquid to solid results in change of the flow mode from ohmic to convective and more rapid acceleration of the polymer jet that are turning to nanofibers now. The obtained nanofibrous scaffolds should have the potential to adsorb proteins and provide the required environment for cell growth (Tariverdian et al., 2019). Nano fibrillar structure of some of the structural elements of the body, like collagen type I in bone ECM can be imitated by this method. One of the positive points of electrospinning is its variety in raw materials selection and the morphology and porosity that it results in. Yang et al. (Yang et al., 2009) showed that the calcium deposition and alkaline phosphate activity of cells in an electrospun scaffold made up of polycaprolactone (PCL) and chitosan are improved. The feasibility of nanofibrous scaffolds modification through incorporation with

bioactive agents is another positive feature of electrospinning (Tariverdian et al., 2019).

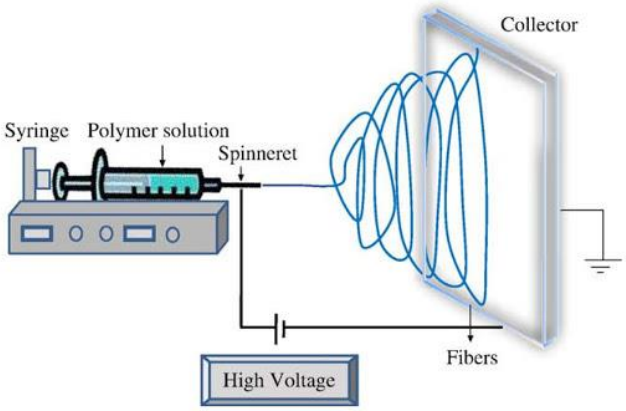

Figure 7. Electrospinning Diagram 1(Bhardwaj & Kundu, 2010)

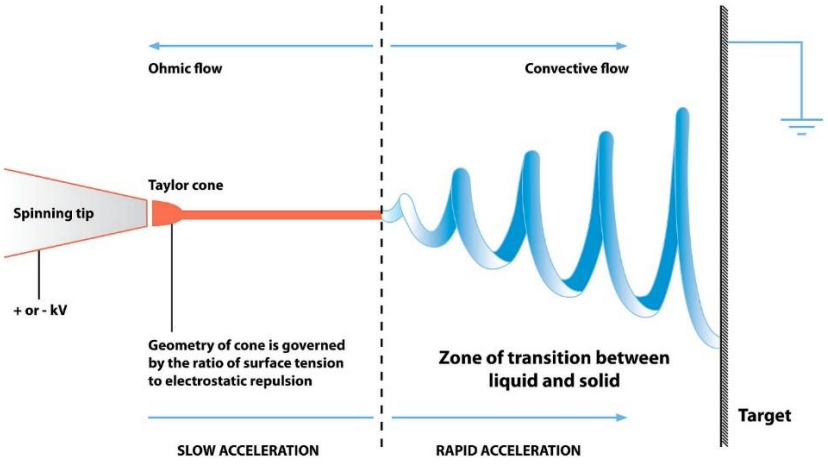

Figure 8. Electrospinning Diagram 2 (Joanna Gatford, The New Zealand Institute for Plant and Food Research)

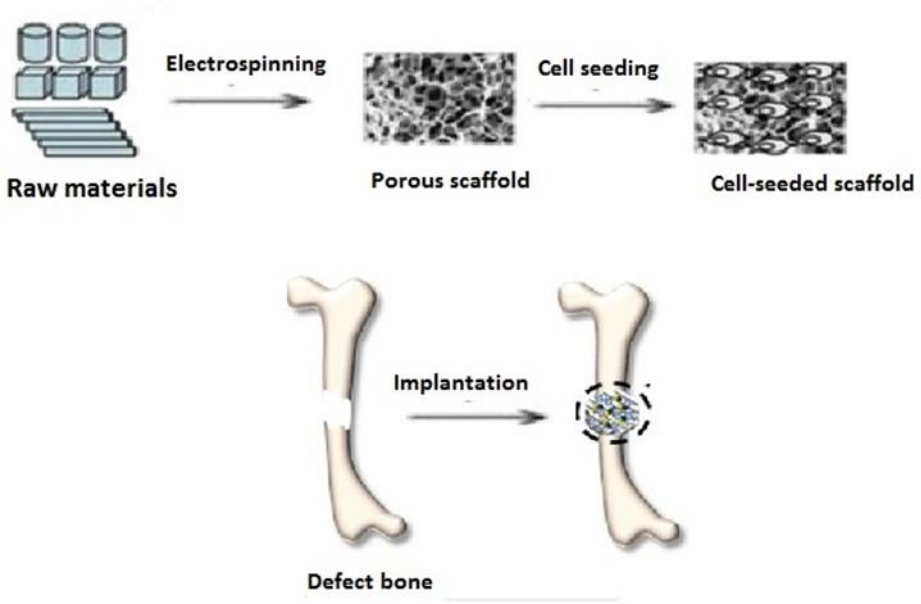

Figure 9. The schematics of fabrication and placement of a bioactive porous bone scaffold followed by the cell seeding(Sefat et al., 2019)

1.2.3.1 Optimum electrospinning conditions

Major setting parameters important in electrospinning are polymer solution properties, flow rate, voltage, and tip to collector distance which all need to be optimized. Polymer solution effective properties include solution viscosity, concentration, conductivity, and surface tension. Molecular weight and architecture of the polymer effect the properties of the solution. It is worth mentioning that there are ambient parameters such as temperature and weather humidity that can have an impact on the process and result of the electrospinning.

1.2.4 Aim of the study

In this study it is aimed to synthesize and compare HA and FHA to develop and investigate FHA and PEEK based composite electrospun scaffolds that are suitable

for bone tissue engineering applications. Although there were a few studies in literature on electrospinning of sPEEK, there were yet no study combining HA and/FHA with sPEEK in electrospinning process to obtain scaffolds for BTE purpose. Therefore, all characterizations of composite scaffolds as well as optimizations of composite scaffold electrospinning conditions will contribute new outcomes and information to the literature in this research area.

CHAPTER 2

MATERIALS AND METHODS

2.1 Materials

Polyether ether ketone (PEEK) (Victrex), Sulfuric acid 95%-97% (Merk), N,N-dimethylacetamide (DMAc) (Sigma Aldrich) were used to prepare sPEEK solutions; for preparation of phosphate-buffered saline (PBS), and simulated body fluid (SBF), and synthesis of HA and FHA, ammonium fluoride (NH_4F) (Merck, Germany), Calcium nitrate tetrahydrate ($Ca(NO_3)_2.4H_2O$) (Merck, Germany), diammonium hydrogen phosphate ($(NH_4)_2HPO_4$) (Merck, Germany), sodium chloride (NaCl) (Merck, Germany), sodium bicarbonate ($NaHCO_3$) (Merck, Germany), potassium chloride (KCl) (Merck, Germany), dipotassium hydrogen phosphate trihydrate ($K_2HPO_4.3H_2O$) (Merck, Germany), magnesium chloride hexahydrate ($MgCl_2.6H_2O$) (Merck, Germany), 1.0M hydrochloric acid (HCl) (Merck, Germany), calcium chloride ($CaCl_2$) (Merck, Germany), sodium sulfate (Na_2SO_4) (Merck, Germany), TRIS (Bio-Rad), disodium hydrogen phosphate dihydrate ($Na_2HPO_4.2H_2O$) (Fluka, USA) and dipotassium hydrogen phosphate (K_2HPO_4) (Merck, Germany) were used.

Utilized material for cell culture studies were fetal bovine serum (FBS) (Biological Industries, USA), high glucose Dulbecco's modified Eagle medium (DMEM) (Merck, Germany), penicillin/streptomycin (Biological Industries, USA), Trypsin, Trypan blue, and AlamarBlue™ (Invitrogen, USA). Furthermore, for cell fixation, paraformaldehyde powder (Sigma, USA), HCl (Merck, USA), hexamethyldisilazane (Sigma, USA), and 1 N NaOH (Merck, Germany) were utilized.

2.2 Methods

2.2.1 Synthesis of HA and FHA

Microwave irradiation method was used to make HA nanoparticles. Calcium source $Ca(NO_3)_2.4H_2O$ (0.2 mole) and phosphate source $(NH_4)_2HPO_4$ (0.12 mole) were dissolved in 200 mL of distilled water separately. Phosphate solution was dropped in the calcium solution. While mixing a previously made ammonia solution was slowly added to keep the pH at desired levels. Then the obtained mixture was stirred at 600 rpm for 30 min at room temperature followed by exposure to microwave irradiation at 800 W for 15 minutes. At last, the mixture was filtrated by filter paper and thoroughly rinsed with distilled water until fully neutralized. Ultimately, it was air dried overnight at 80˚C in the oven. Dried HA was crushed by pestle and mortar and the obtained powder was sintered at 1100˚C for 1h. To obtain uniform small graine powder, it was passed through 80-micron sieve.

FHA was obtained with adding a 0.1 N Ammonium fluoride (NH_4F) in relation to the Hydroxyl group in the final structure to the solution containing the phosphate source, and the rest of the process was identical.

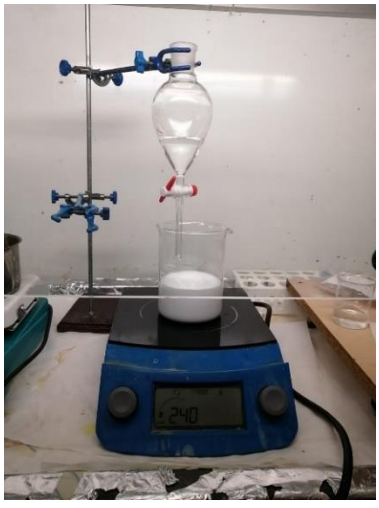

Figure 10. Picture of calcium solution titration by phosphate solution, an stage of HA synthesis

2.2.2 Characterization of HA and FHA

Characterization of HA and FHA powders was carried out by Scanning electron microscopy (SEM), Energy Dispersive X-ray (EDX), X-Ray Diffraction analysis (XRD) and Fourier-Transform Infrared Spectroscopy (FTIR) analysis at Central Laboratory (MERLAB). SEM is used to investigate surface topography and EDX was done for elemental analysis; both were carried out by QUANTA 400F Field Emission SEM.

XRD is used for determining the crystalline structure and FTIR shows the functional groups in the material. A diffractometer (Rigaku Ultima-IV, Japan) with Cu-Kα radiation was used for the XRD analysis at 40 kV and 30 Ma. The range of scan was between 10˚ and 90˚ in 2θ. The duration time per scan ratio(scan step) was 1 deg/min, and the step/sampling step ratio was 0.02 deg. Using the International Centre for Diffraction Data database, the phases present in the sample were determined (ICDD).

For FTIR analysis, a spectrometer was utilized. Fifty scans per sample were performed at wavenumbers ranging from 4000-400 cm^{-1}, with a 4 cm^{-1} resolution. For measurement, the samples were crushed with a pestle and mortar and mixed with KBr at a 1:10 ratio. The spectra of the samples were adjusted for background and atmosphere noise.

2.2.3 Sulfonation of Poly(ether ether ketone)

PEEK in the powder form was sulfonated by dissolving in sulfuric acid (95-97%) in a glass flask. Each gram of PEEK requires 20 mL of sulfuric acid (5/95 w/v). To ensure a homogeneous sulfonation, PEEK was completely dissolved in Sulfuric acid at room temperature in about an hour, just before increasing the reaction temperature to the desired temperature (55˚C). After stirring under reaction conditions for a certain amount of time, the flax was put in ice water while stirring to terminate the temperature dependent reaction. Then solution was put in deionized water to obtain

solid sPEEK polymers and remove the sulfuric acid. Obtained material was washed with deionized water till the washing water's pH was above 5 (or 5.5 depending on the pure water pH) to make sure the residual Sulfuric acid was washed off(Huang et al., 2001). A noteworthy point is that after a few times of trial it was concluded that leaning the flask's opening towards a stirring full of water beaker's inner wall in a manner that the solution would enter the water drop by drop sliding down on the inner surface and enter the water by being released from adhesive and cohesive forces is a very efficient way of performing this procedure. Since it provides a very big surface to volume ratio and prevents spherization of the drops. Another important point is that the sulfonation is very sensitive to the reaction temperature as only one degree fluctuation could lead to different solubility properties in the electrospinning. Finally, the obtained sample was airdried at 60˚C overnight(Huang et al., 2001).

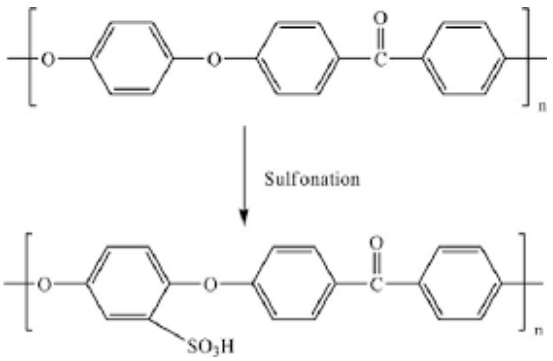

Figure 11. Sulfonation of PEEK(Mohsenpour et al., 2018)

2.2.3.1 Determining the sulfonation degree

The sulfonation degree of SPEEK was determined by the back titration method. For the back titration 0.2 gram of dried sample was added to 100mL of 0.01M sodium hydroxide aqueous solution and stirred for 3 days to make sure it has completely turned to its sodium salt (SPEEK-H to SPEEK-Na)(Huang et al., 2001).

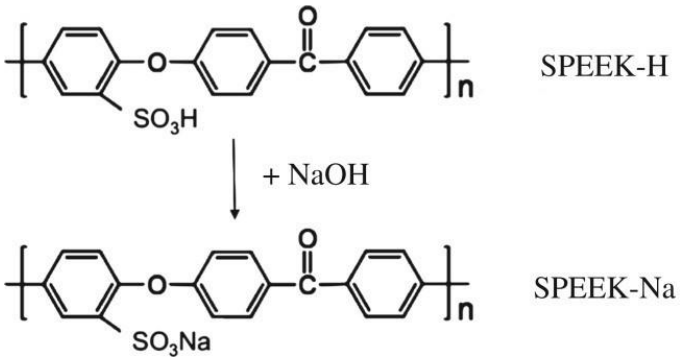

Figure 12. Turning SPEEK to SPEEK-Na(Wang et al., 2019)

2.2.3.2 Back-titration of NaOH Solution

Since the NaOH solution has been partially neutralized by the hydrogens released from -SO_3H groups of sPEEK, a back-titration of the NaOH solution can show the amount of -SO_3 groups initially present in the structure. Since each -SO_3H group has one acidic hydrogen to neutralize NaOH, and we know the molarity of -OHs in the pure NaOH solution, by calculating the molarity of hydrogens needed to back-titrate the partially neutralized (by sPEEK) NaOH solution to neutral PH we can determine the molarity of acidic hydrogens released from the sPEEK which is equal to the molarity of the -SO_3H groups.

Back-titration is carried out with dilute sulfuric acid with a molarity of 0.003M. Since Sulfuric acid is a dibasic acid, the molar quantity of the -SO_3 groups can be calculated by the Equation 1(Huang et al., 2001):

$$N_{SPEEK\text{-}H} = (MV)_{NaOH} - 2(MV)_{sulfuric\ acid}$$

(M is Molarity and V is Volume) (1)

2.2.3.3 Calculation of Degree of Sulfonation

The degree of sulfonation (DS) can be calculated by the following Equation 2:

$$\frac{\text{molar number of the (PEEK}-\text{SO3Na) unit}}{\text{molar number of the (PEEK}-\text{SO3Na) unit} - (\text{molar number of the (PEEK} - \text{SO3Na) unit} + 1 \text{ molar number of the PEEK unit})} \quad (2)$$

The molar number of the PEEK–SO_3Na unit (N1) per 1g sulfonated PEEK is:

$$N1 = 0.001 * IEC \quad (IEC= Ion\text{-}Exchange\ Capacity) \quad (3)$$

The molar number of the PEEK unit (N2) in 1g sulfonated PEEK is:

$$N2 =(1 - 0.001 * IEC * M1)/M2 \quad (5)$$

M1 and M2 are molecular weights of sPEEK –SO_3Na unit and the PEEK unit respectively:

$$M1 = 390\ (Da) \quad M2 = 288\ (Da) \quad (6)\ ,\ (7)$$

Inserting the numbers and combining the equations 2, 3, and 5 gives Equation 8(Huang et al., 2001):

$$SD =288 * IEC/(1000 - 102 * IEC) \quad (8)$$

2.2.4 Optimizing Sulfonation degree and determining the best solvent and SPEEK/solvent ratio

Intermolecular bonding of polymers is stronger in crystalline form which leads to higher mechanical strength. Sulfonation decreases crystallinity reducing the mechanical strength.

To find the right solvent and optimize Sulfonation degree of the sPEEK, a feedback system was used. The primary principle was to find the solution able to dissolve SPEEK with the least sulfonation degree within the range of 10 to 20 percent (as the

least acceptable practical ratio) among the solvents known for dissolving sPEEK while having the least sulfonation degree for sPEEK. Previous research reported that the minimum sulfonation degree required for PEEK to be dissolvable in organic solvents at room temperature is above 40% of sulfonation(Zaidi et al., 2000). 55˚C was chosen as the reaction temperature since it is faster and keeps the initial linear increasing phase until higher sulfonation degrees. So samples with different sulfonation reaction times were prepared to match the approximation(Huang et al., 2001) of 40%, to 100% by 10% intervals. On the other hand, to detect the best solvent, HFIP, Chloroform, DMSO, DMAc, DMF and DCM were tested with different ratios of aforementioned sPEEKs(Y. Liu et al., 2008).

2.2.5 Preparation of the sPEEK Scaffolds

Wet electrospinning method was used to obtain the scaffolds in the setup shown in Figure 16. The SPEEK solution was put into a syringe which's tip was flattened before. The tip of the syringe was linked to the voltage source (ES30, Gamma High Voltage Research, Inc., USA) by a clipped wire. The syringe was fixed in a pump (New Era Pump Systems, USA) so it is pushed in a certain set rate and can be adjusted with the voltage intensity from the power source. The correct setting of tip to collector distance, voltage and pumping rate was optimized, and electrospinning was done to obtain 3D fibrous sPEEK scaffolds. A rotating big size Petri dish filled with 96% Ethanol was used as the collector. The tip to collector distance was fixed at 12cm. Flow rate was altering between 0.1 mL/hr to 0.15 mL/hr depending on the solution type. The voltage was set on 22kV during all the experiments. Seven different groups of scaffolds were prepared by electrospinning sPEEK solution with different amounts of incorporated HA or FHA. The groups were 20% SPEEK, 20%SPEEK + 1%HA, 20%SPEEK + 2.5%HA, 20%SPEEK + 5%HA, 20%SPEEK + 1%FHA, 20%SPEEK + 2.5%FHA, 20%SPEEK + 5%FHA. Obtained scaffolds were put in vacuum oven for drying.

During electrospinning experiments, it was noticed that storage time effects sPEEK's scaffold formation. Therefore, it is highly important to use freshly made sPEEK as the kept ones after some time in order of a week lose their ability.

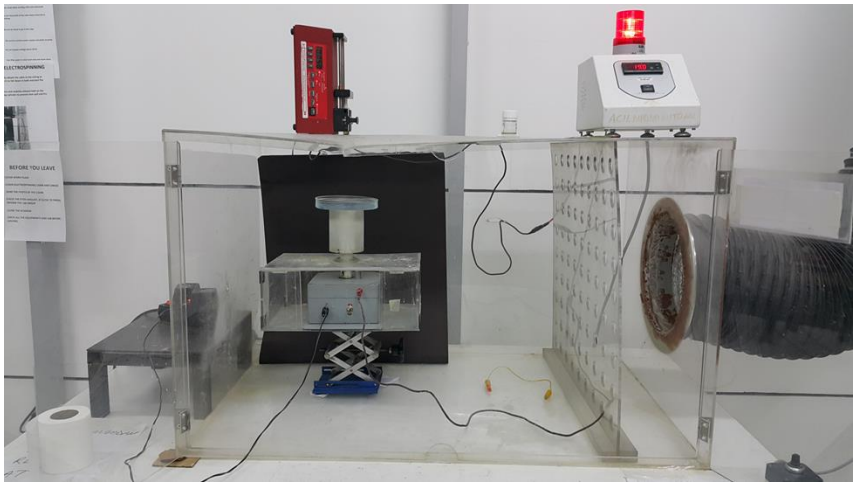

Figure 13. Wet electrospinning set up

2.2.6 Scaffolds Characterizations

For this section SEM, EDX, FTIR, bioactivity test, and in vitro degradation assay were done.

Bioactivity test or Simulated Body Fluid test (SBF) is done by incubating the samples in SBF solution at 5% CO2 and 37°C in a carbon dioxide incubator (5215 Shel Lab., Cornelius, OR, USA). The weight changes were measured at certain time points. Furthermore, at the end of each time point dried samples were analyzed by SEM and EDX analysis to check the apatite layer formation on their surface. SBF solution was prepared in accordance with modified Kokubo's solution(Kokubo et al., 1990). To this end various components were added to 500 mL distilled water at the room temperature while stirring in the amounts and the order as specified in Table 3. The weighing and addition of each component was done immediately. The amount of HCl added is about 90% of the total required amount and the rest will be added to adjust the pH to 7.40 after putting the stirring solution in a water bath at 37˚C.

Table 3. Components of SBF solution (1 Liter)

Order	Chemicals	Amounts
1	NaCl	7.996 g
2	$NaHCO_3$	0.350 g
3	KCl	0.224 g
4	$K_2HPO_4 \cdot 3H_2O$	0.228 g
5	$MgCl_2 \cdot 6H_2O$	0.305 g
6	1M-HCl	40 mL
7	$CaCl_2$	0.278 g
8	Na_2SO_4	0.071 g
9	$H_2NC(CH_2OH)_3$(Tris)	6.057 g

It is important to make and keep the SBF solution in polyethylene or polystyrene container and between 5˚C to 10˚C before use. If any precipitation is observed, it should be reproduced.

Scaffolds of each group (n=4) weighing approximately 0.005 g were put in 10 mL PBS in 15 mL falcon tubes. Falcons were put in water bath shaking at 37˚C. The dry weight of scaffolds was measured prior to this, and wet weight of scaffolds were measured after 1, 7 and 14 days. Additionally dry weight of scaffolds was measured at day 14.

For preparing PBS required amounts of NaCl, KH_2PO_4, Na_2HPO_4, and KCl were mixed (Table 4.) in 800 mL of distilled water(*Molecular Cloning: A Laboratory Manual.*, n.d.). Using HCl the pH was adjusted to 7.4 and the total volume was completed to 1 liter by adding more water. Then it was autoclaved to be sterilized.

Table 4. Components of PBS solution (1 Liter)

Chemicals	Amounts
NaCl	8 g
KCl	0.2 g
Na_2HPO_4	1.44 g
KH_2PO_4	0.24 g

During the incubation, pH changes were measured in the solutions at each time point as well. Finally, scaffolds were sent to SEM and EDX analysis to observe apatite layer formation and fiber diameter measuring.

For invitro degradation tests samples were put into PBS solution (0,01 M, pH 7.4) in similar manner to SBF in bioactivity test. Dry and wet weights were measured to calculate swelling ratio (SR) and weight loss at the end of each time period and pH changes were also measured. Swelling ratio is measured by the formula mentioned in Equation (4)(Nokoorani et al., 2021):

$$SR(\%) = \frac{Ww - WD}{WD} \times 100 \quad (4)$$

W_w : Wet weight after removal of excess solvent on scaffold, and W_D : Dry weight.

2.2.7 Cell culture Experiments

Human osteosarcoma cell line (Saos-2) (ATCC, USA) is used for cell culture experiments. Media was prepared by using a high glucose Dulbecco's modified Eagle medium (DMEM), supplemented with 10% (v/v) FBS and 1% penicillin/streptomycin.

The cells were seeded in a 75 mL flask and incubated at 37°C in a carbon dioxide incubator (5% CO2, 5215 Shel Lab., Cornelius, OR, USA) until the surface of the flask was about 80% confluent (covered with cells, indicating that the cells are in the log phase of growth). Then the cells were removed by treating with Trypsin and counted under light microscope after 1:1 Trypan Blue addition to an aliquot of the media containing the cells; afterwards the cell solution was diluted with media to reach the desired concentration of cells for seeding in the wells or on the scaffolds.

2.2.7.1 HA and FHA cytotoxicity test

Cytotoxicity of HA and FHA powders were measured by indirect cytotoxicity test. Saos-2 cells were seeded at 10^4 cells/well density in 96 well plates 24 h before starting

the experiment. HA and FHA powders were sterilized by heating up to 200˚C for 2 h. Then the powders were put in media with a 0.2 gr/mL concentration and incubated in water bath at 37˚C for 24 h. There were HA, FHA, and control groups, HA and FHA groups each were in 3 different concentrations of 1(exact extraction media), ½ (extraction media diluted to its half concentration with fresh media), and ¼.(Extraction media diluted to its one fourth concentration with fresh media); there was also an only media group (without extraction) as control. 3 samples were used for each group. Alamar blue cell viability test was used to measure the cytotoxicity of the powders. Seeded scaffolds were kept at 37°C in the carbon dioxide incubator (5% CO_2, 5215 Shel Lab., Cornelius, OR, USA) and Alamar blue test was performed every day for 3 consecutive days with a similar protocol to the one described in the cell viability test of scaffolds.

2.2.7.2 Alamar Blue cell viability test of scaffolds

Scaffolds were cut to fit 96 wells and treated with ethanol for two hours and each side was exposed to UV light for 30 minutes, then they were placed in a sterile 96 well plate and then previously grown cells (10^4 cells/well) were planted by the cell suspension on to each scaffold. Control groups (cells seeded in wells without scaffolds) and blank groups (only media) were present. Media for cell culture experiments were refreshed in every 3rd day. Seeded scaffolds were kept at 37°C in the carbon dioxide incubator (5% CO_2, 5215 Shel Lab., Cornelius, OR, USA) and Alamar Blue test was performed on them at the end of first, fourth and seventh days of incubation. To perform this test, Alamar Blue solution was prepared by adding 10% Alamar Blue to 90% phenol red-free DMEM. Then, 100 µL of it was put in each well and kept for 6 hours in the incubator. Then the Alamar solution was transferred to a new 96 well plate and the absorption of each well was read by a spectrophotometer (µOuantTM, Biotek Instruments Inc., USA) and recorded using the ELISA software program (Atlanta, USA) at 570 nm and 600 nm. Meanwhile wells were washed with PBS, and fresh relative media replaced the extracted Alamar from the wells and the plate was put back into incubator till the next time point. Due to light sensitivity, all

Alamar Blue experiment steps were conducted at dark. To analyze cell viability, adhesion and spreading on the scaffolds, at the end of day 7 the cells were fixed on scaffolds by immersing in paraformaldehyde solution (4%w/v) prepared with PBS for 10min and then being washed with pure PBS after treatment. To prepare 4% (w/v) paraformaldehyde, paraformaldehyde powder was dissolved in PBS in the proper amount according to the 4% ratio and 1 N NaOH was added to obtain a clear solution. Eventually by using HCl dilute solution the pH of the solution was set to 6.9. After removing excess PBS samples were dehydrated by being immersed in different gradually increasing concentrations of ethanol solution (20% to 100% with 10% increase each time) for 10min each. After removal of ethanol, hexamethyldisilazane treatment was done and samples were air dried under hood. Cells on the surface of the scaffold were analyzed by SEM.

2.2.7.2.1 Alamar Blue Data Analysis

In the assay reduction of Alamar Blue is measured as an indicator of cellular activity relatable with cellular growth. Then it is compared to the blank of media only. To fulfill this purpose, following formula is used (Equation 5)(*Measuring Cytotoxicity or Proliferation - AlamarBlue Assay Protocol | Bio-Rad*, n.d.):

$$\frac{(O2\ x\ A1) - (O1\ x\ A2)}{(O2\ x\ P1) - (O1\ x\ P2)} x100 \quad (5)$$

Where:

O1 = molar extinction coefficient (E) of oxidized Alamar Blue (blue) at 570 nm*

O2 = E of oxidized Alamar Blue at 600 nm

A1 = absorbance of test wells at 570 nm

A2 = absorbance of test wells at 600 nm

P1 = absorbance of positive growth control well (cells plus Alamar Blue but no test agent) at 570 nm

P2 = absorbance of positive growth control well (cells plus Alamar Blue but no test agent) at 600 nm

The control group's reduction was considered 100% at each testing time point and then for others relative cell viability was obtained, thus the results of each testing time point is only comparable to the others at the same test.

CHAPTER 3

RESULTS AND DISCUSSIONS

3.1 Characterization Results and Cytotoxicity of Synthesized Minerals (HA and FHA)

3.1.1 FTIR Analysis Results

Typical HA structure is achieved by the presence of absorption bands matching the reference pattern of phosphate and hydroxyl groups of HA in the FTIR spectra given in Figure 17. Obviously, phosphate groups are always present in the FTIR spectra of HA, and usually are divided into symmetric stretch, asymmetric stretch and bending vibrational modes. The symmetric stretch mode corresponding to PO_4^{3-} is distinguishable at the absorption band at 961 cm^{-1}, asymmetric stretch mode corresponding to PO_4^{3-} is represented at the absorption bands at 1087-598-560-474 cm^{-1}, and bending mode corresponding to PO_4^{3-} is seen at 1022 cm^{-1}. The absorption band at 628 cm^{-1} is present due to the vibration of the hydroxyl group(Jaber & Kovács, 2019)·(*An Investigation of Microstructure , Microhardness and Biocompatibility Characteristics of Yttrium Hydroxyapatite Doped With Fluoride a Thesis Submitted To the Graduate School of Natural and Applied Sciences of Middle East Technical University By Sidika M*, 2010).

It's noticeable that absence of remarkable absorption bands in 3500 cm^{-1} to 4000 cm^{-1}, shows that the sample has been properly dried.

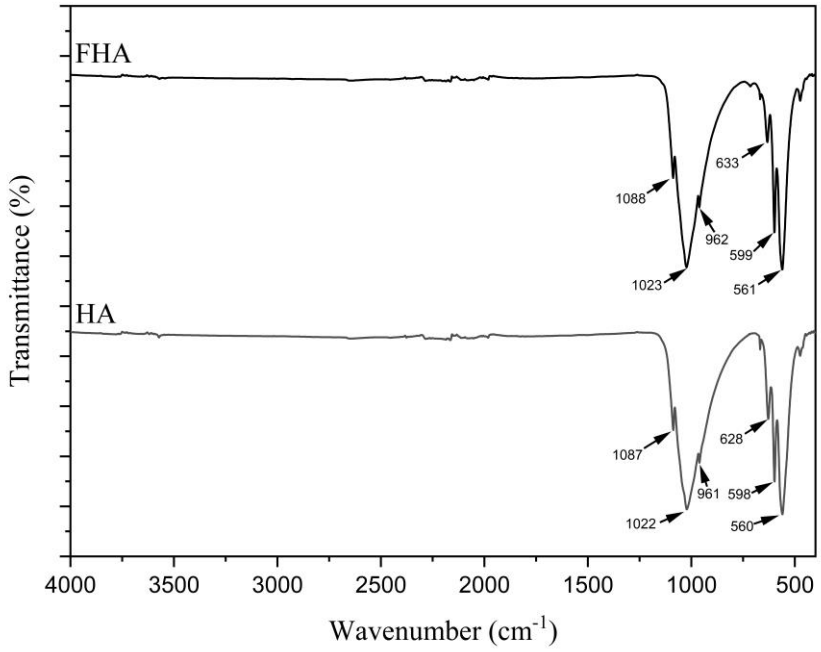

Figure 14. Pure HA and 10% Fluoride doped FHA powder FTIR diagram

Similar elaboration is true for the FHA. Furthermore, shifts and the changes in intensity of absorption bands in comparison with HA suggests a successful doping. The FHA sample is 10% fluoride doped HA (10% of (OH) group in HA ($Ca_{10}(PO_4)_6(OH)_2$)).

In comparison of FHA to HA, majority of absorbance bands have shifted towards higher wavenumbers. For example, $(OH)^-$ liberation band is observable at 628.32 cm^{-1} for HA and at 632.50 cm^{-1} for FHA. The intensity of $(OH)^-$ liberation band has decreased in FHA as well, indicating successful substitution of F^- to $(OH)^-$. Another indicator of such successful substitution is the curve in the proximity of $(OH)^-$ stretching band (3572.66 cm^{-1}) in HA which almost vanishes in the FHA sample.

3.1.2 XRD Analysis Results

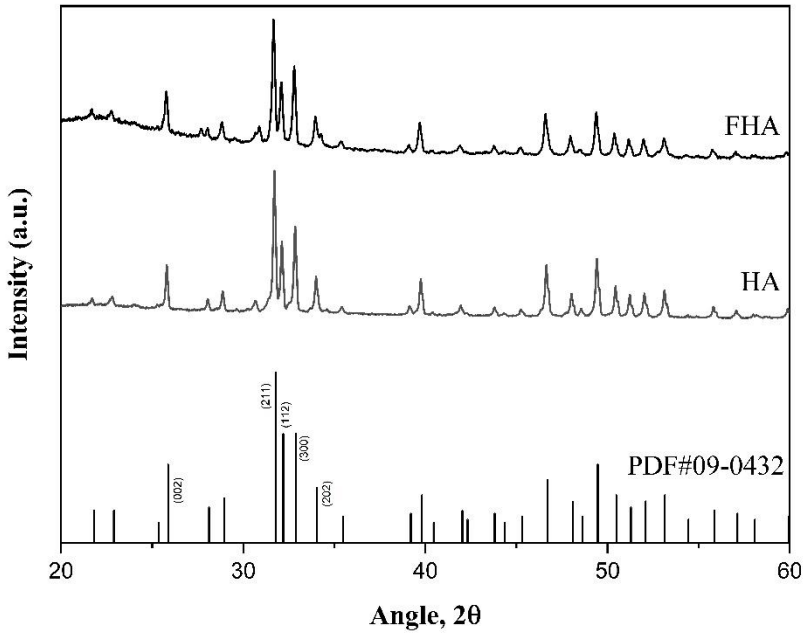

Figure 15. HA and FHA XRD patterns

As seen in (Figure 17.) XRD pattern of the HA sample shows great overlapping with International Committee for Diffraction Data (ICDD) powder diffraction file for HA (PDF NUM: 09-0432)(*JADE® Pattern Converter*, n.d.).

Great overlap with ICDD file for HA is observed. Negligible amounts of 210 beta-TCP (β-TCP) (PDF NUM: 090348) was also detected. The intensity of the absorption peaks has increased as expected, since the F^- ion increases crystallinity, this suggests a successful doping.

3.1.3 SEM Analysis Results of HA and FHA particles

The synthesized HA and FHA particles were investigated by SEM and presented in Figures 18 and 19. FHA particles have more coagulation, than HA ones. HA particles are more dispersed, and they seem to be larger than FHA ones. Both FHA and HA had homogenous particles in terms of size and shape.

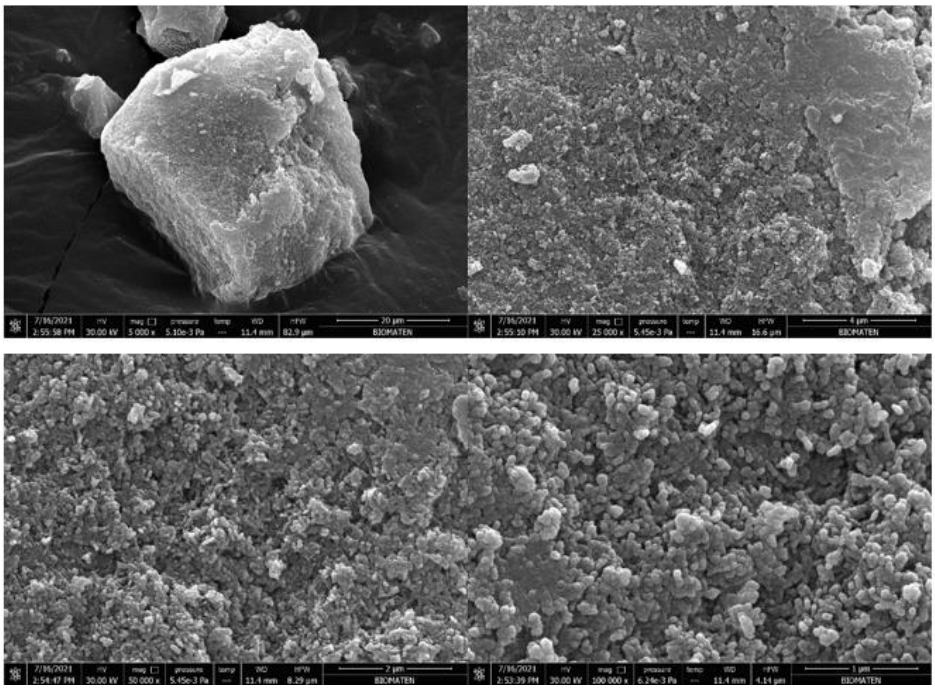

Figure 16. SEM images of HA particles in different magnifications

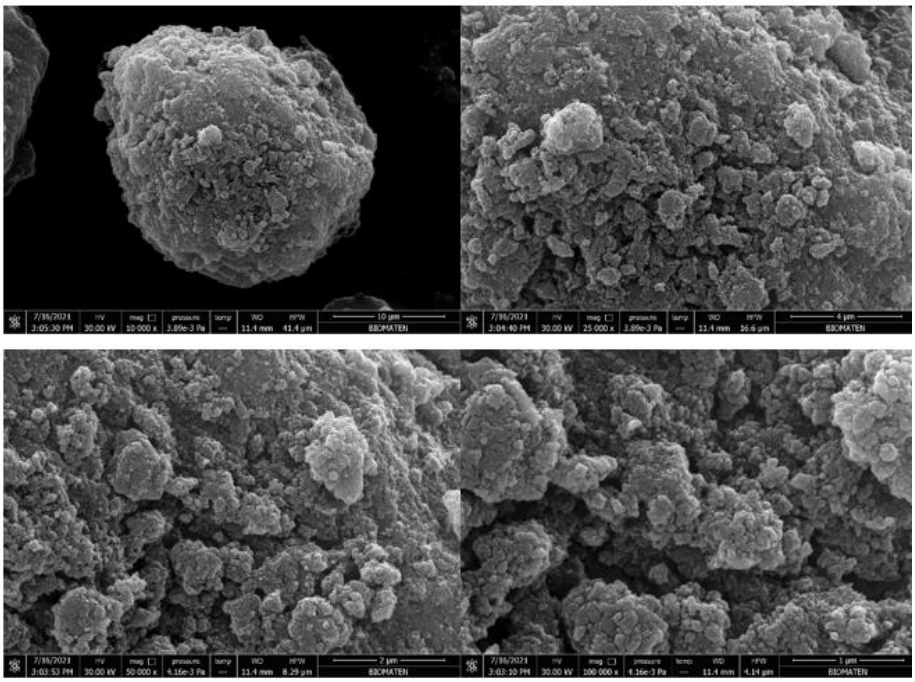

Figure 17. SEM images of FHA particles in different magnifications

SEM image of both HA and FHA suggested that particles were quite small (app. 100-200 nm) in size and therefore, could be used for electrospinning within polymer solution.

3.1.4 EDX Analysis Results of HA and FHA particles

EDX results show successful doping of Fluor into the HA structure. An example of the elemental analysis results for each HA and FHA powders is demonstrated below:

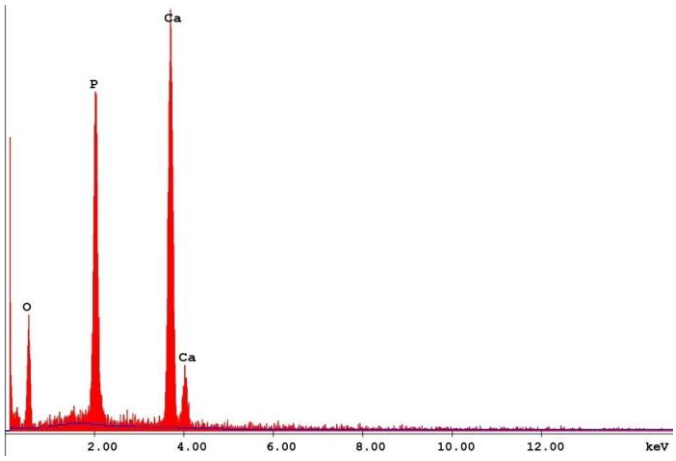

Figure 18. EDX spectrum of HA

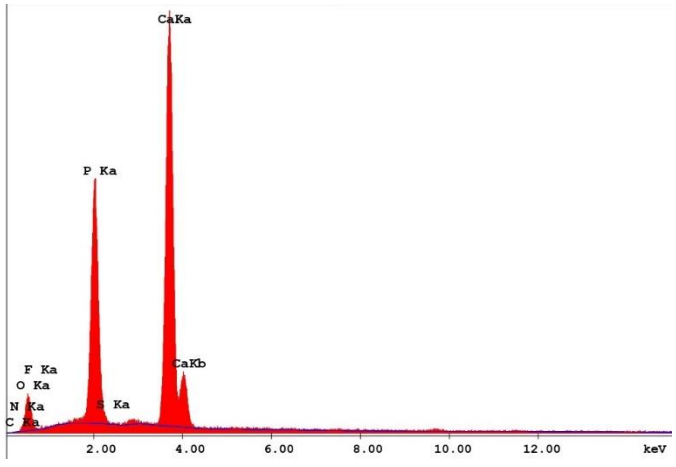

Figure 19. EDX spectrum of FHA

Table 5. Examples of EDX elemental analysis results for HA and FHA particles

	HA		FHA	
Element	Wt %	At %	Wt %	At %
C	0.00	0.00	0.00	0.00
N	0.00	0.00	0.90	1.59
O	34.11	54.05	34.71	53.58
F	0.00	0.00	1.49	1.94
P	23.04	18.85	22.48	17.93
S	0.00	0.00	0.42	0.33
Ca	42.85	27.10	40.00	24.64
Total	100.00	100.00	100.00	100.00
Ca/P ratio	1.86	1.44	1.78	1.37

3.1.5 HA and FHA indirect cytotoxicity

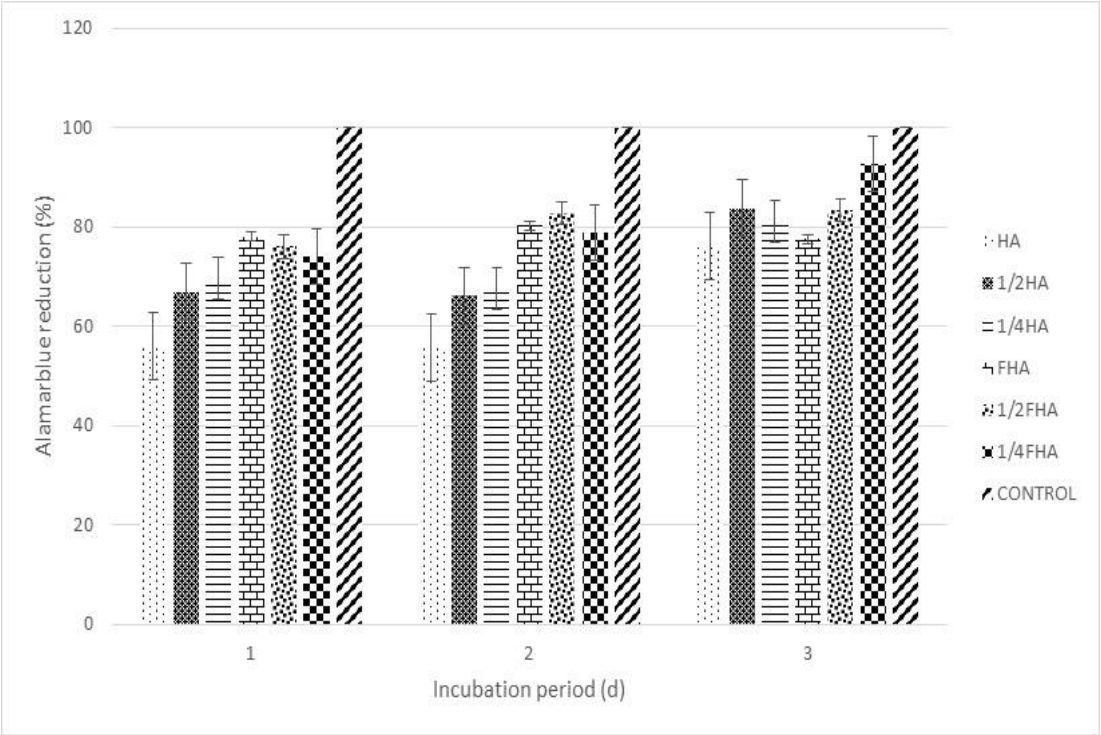

Figure 20. HA and FHA indirect cytotoxicity by Alamar blue reduction test in day 1, 2, and 3.

At the first two days even though ingroup differences are insignificant but the difference between HA and FHA groups is quite evident and shows that FHA is significantly less cytotoxic at the same concentrations. Previous research has shown that HA can be cytotoxic and anti-proliferation based on cell type for instance for several types of cancer and some other cell types(Yuan et al., 2010)·(Sun et al., 2020). The trend in groups in the experiment show that doping Fluor for as much as 10% of (OH) molarity in HA significantly reduces its toxicity. Furthermore, on the third day which is the day after the doubling-time period (Saos-2 cell line's doubling time is 35-40h)(*Characterization of a Human Osteosarcoma Cell Line (Saos-2) with Osteoblastic Properties | Cancer Research | American Association for Cancer Research*, n.d.), even though the growths in the FHA group were comparable for the 3 concentrations of the powders in the applied media, ¼ FHA shows significantly better results than ¼ HA and all others especially on the 3rd day; it is almost the same

as the control group. This is consistent with the previous research on the matter that up to a certain concentration addition of fluor to the structure of HA is beneficial for cell proliferation(Nasker et al., 2019).

3.2 PEEK/sPEEK

According to initial experiments for sPEEK, DMAc was chosen as the solvent to carry on the electrospinning due to having the clearest solution in the same ratios of solute.

sPEEK was dissolved in DMAc in 15% and 20% (w/v) and the obtained scaffolds were sent to SEM analysis to verify fibrous structure. During optimization studies, considering bead formation ratio, it was decided to continue with 20% solution. As is known, higher concentration of the solution is better for reducing the beads in the scaffold(Y. Liu et al., 2008).

3.2.1 Sulfonation degree calculation

The sulfonation degree of the produced sPEEK samples were determined by back-titration method. By placing the required amounts of 0.003M sulfuric acid for neutralizing the NaOH solution and taking an average of different batches, the Sulfonation degree for sPEEK made by 2.5 hours sulfonation reaction at 55˚C was calculated to be 72.5 ± 1 percent. Produced sPEEK was dried in oven over night and kept at 4 °C before further characterizations.

3.2.2 FTIR Analysis Results of PEEK and sPEEK

At the backbone of PEEK the stretching vibrations of C=O group is causing the strong band at 1646 cm^{-1}. The 1594 and 1488 cm^{-1} bands are due to stretching vibrations of C=C in the aromatic ring(Gong et al., 2016). Besides that, band around 1200 cm^{-1} was primarily due to the presence of aryl oxide(He et al., 2017).

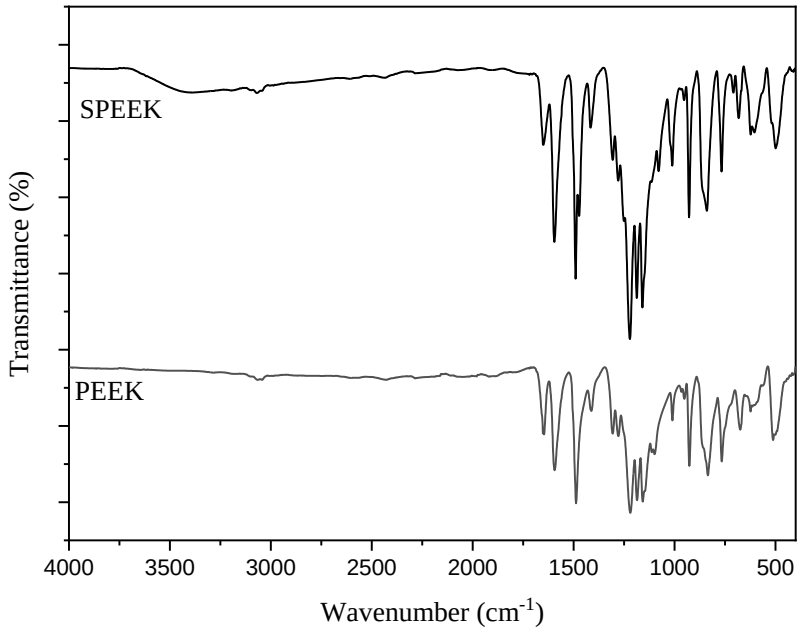

Figure 21. FTIR results of PEEK and SPEEK

After sulfonation, some new characteristic absorption bands are observed: the 1079 and 1011 cm^{-1} bands are respectively indicators of O=S=O and S=O symmetric stretching vibrations. Furthermore, the band at 708 cm^{-1} could be assigned to S-O stretching(Gong et al., 2016). Another noteworthy change was the band at 3388 cm^{-1} caused by –OH. It is a typical sign caused by hydration, suggesting the hydrophilicity of materials was significantly improved during the sulfonation process(Gong et al., 2016).

3.3 Characterization of the scaffolds

3.3.1 Degradation and Bioactivity results

During the degradation study, scaffolds were incubated in PBS for 1, 7, and 14 days in the water bath. Scaffolds weight changes, and the pH values of the media were measured. There was a decrement trend in the weights of the scaffolds indicating degradation (Fig. 22). An immediate decrease of pH at the first day was evident which can be related to release of hydrogen ions from the scaffolds since PEEK was sulfonated. However, pH changes were similar between different bioceramic type and ratio groups (Fig. 23).

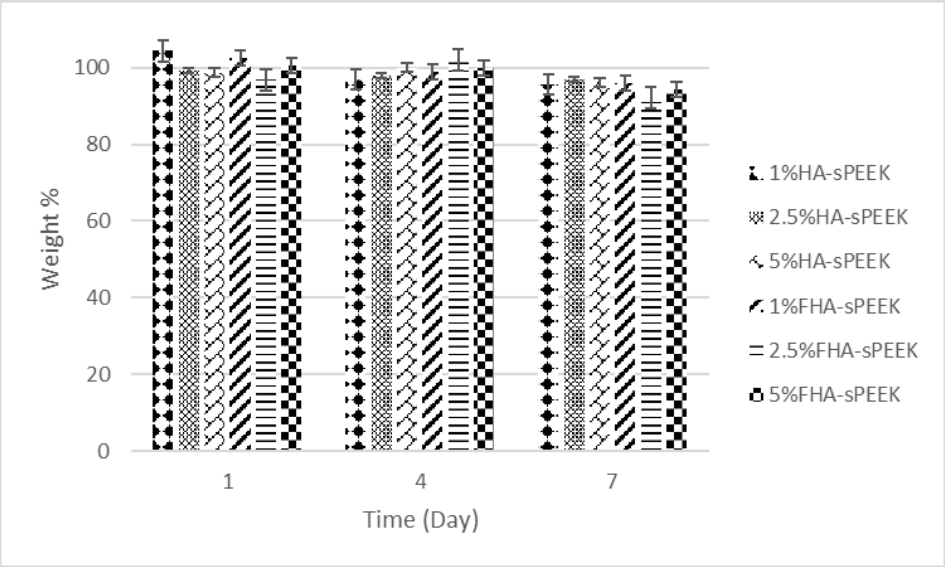

Figure 22. Average weight changes of scaffolds (n=3) in PBS

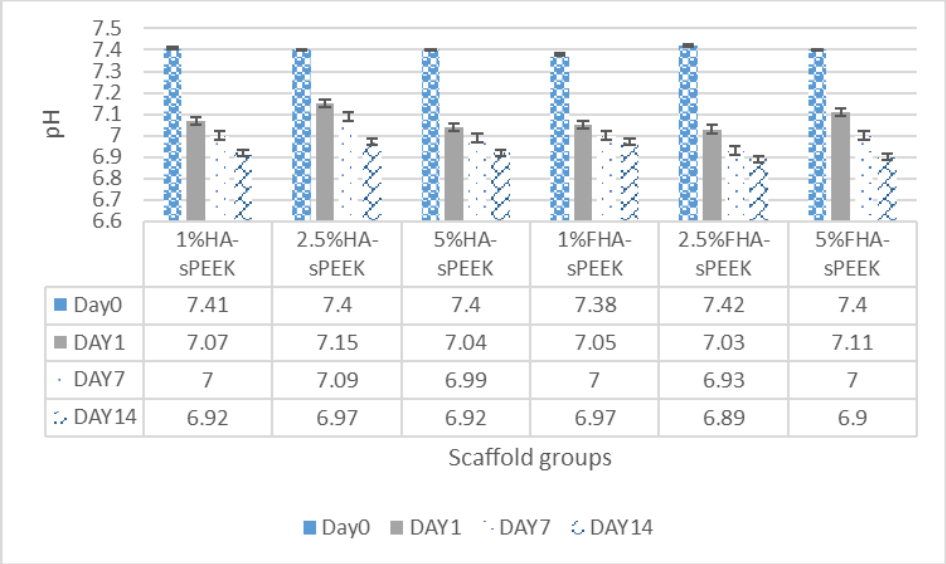

Figure 23. pH values of different scaffold groups during degradation study

Scaffolds were also incubated in SBF, at 37˚C in water bath for 1, 7, and 14 days. Overall, significant changes in the weight of incubated scaffolds were not observed but there was a general slight increment trend especially when compared with degradation results of PBS incubations (Fig. 24). This can be related to mineralization on the scaffolds in SBF media since phosphate ions in PBS interact with positively charged Ca ions in the bioceramics containing HA and make a base for crystallization and apatite layer formation(Dridi et al., 2021).

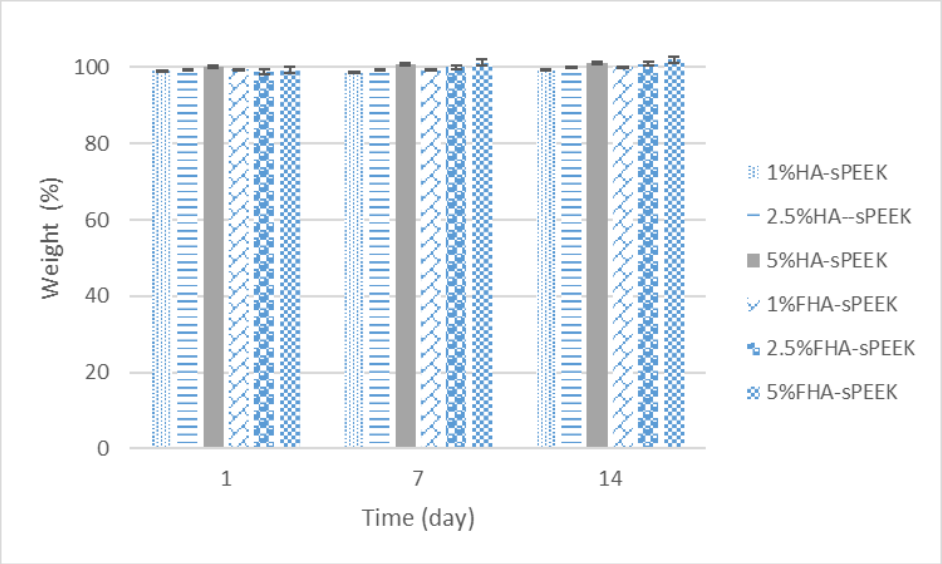

Figure 24. Average weight changes of scaffolds (n=3) in SBF

After drying of 1 sample from each incubation period for each group during bioactivity experiments, samples were sent to SEM analysis. According to SEM results given in Figures 25-30 addition of bioceramics had considerable change on mineral accumulation on the surface of the scaffolds. In Figure 25 a, the fibrous scaffold structure was clear at 1st day. And the fibers were quite homogenous in size. Upon incubation there were some structural changes like enlargement of fibers probably due to swelling with incubation, but there was no recognizable mineral accumulation the surface of scaffolds.

However, mineral deposition on scaffolds were evident with all HA and 1 % FHA including groups especially at 14th day (Figures 25-28 c). Unlikely to this trend at 2.5 % FHA and 5 %FHA 7th day SEM images seemed to have more mineralization (Figure 29-30) than 14 days which might be related with detachment of minerals from surface due to high accumulation after a longer period.

Beside these, in all scaffold groups including bioceramic incorporated ones a considerable change in scaffold microstructure (in addition to mineralization) was noticed. It was thought that addition of minerals contributed to both formation of a denser scaffold interior and a more hydrophilic overall structure which had more swelling related conformational changes upon incubations in aqueous environments.

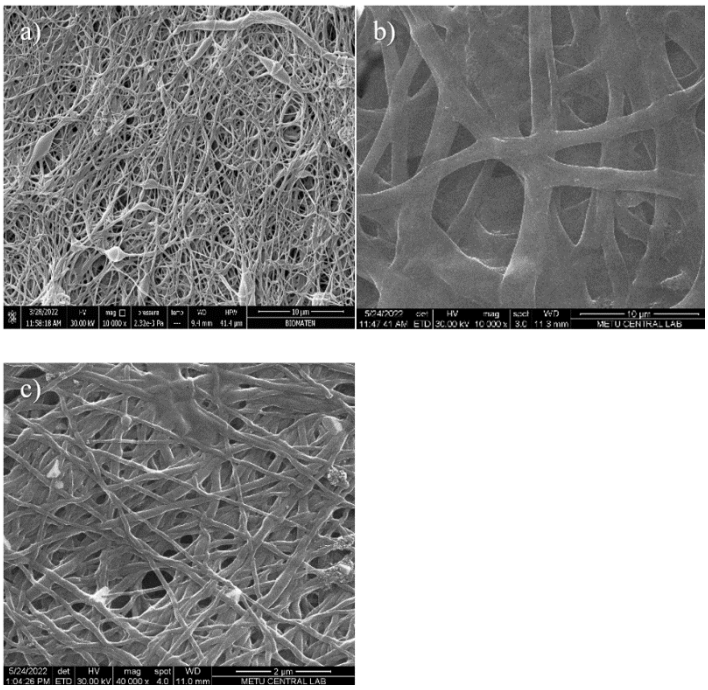

Figure 25. SEM images of sPEEK scaffolds (without bioceramics): a) after 1 day in SBF b) after 7 days in SBF c) after 14 days in SBF

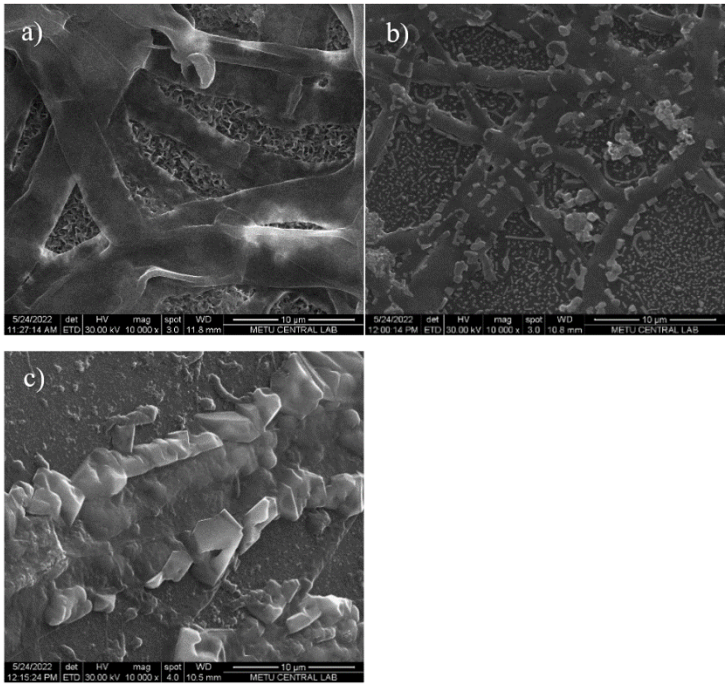

Figure 26. SEM images of 1% HA incorporated sPEEK scaffolds: a) after 1 day in SBF b) after 7 days in SBF c) after 14 days in SBF

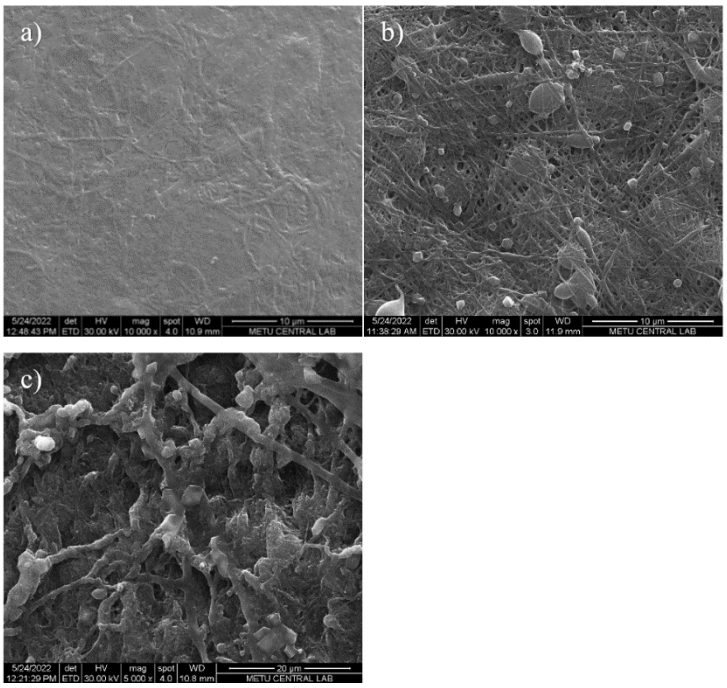

Figure 27. SEM images of 2.5% HA incorporated sPEEK scaffolds: a) after 1 day in SBF b) after 7 days in SBF c) after 14 days in SBF

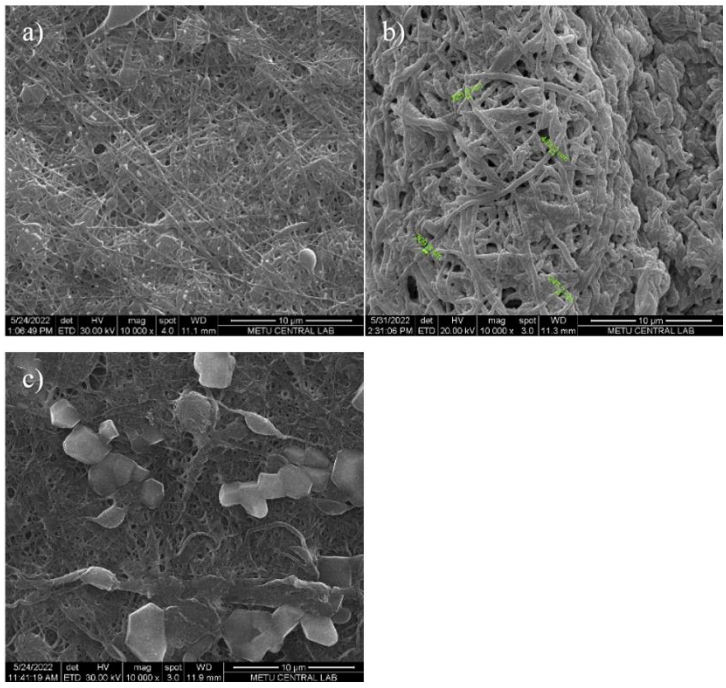

Figure 28. SEM images of 5% HA incorporated sPEEK scaffolds: a) after 1 day in SBF b) after 7 days in SBF c) after 14 days in SBF

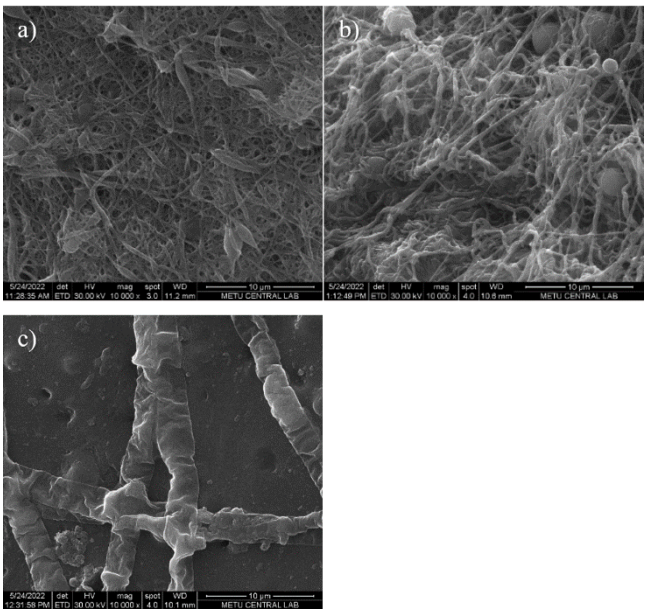

Figure 29. SEM images of 1% FHA incorporated sPEEK scaffolds: a) after 1 day in SBF b) after 7 days in SBF c) after 14 days in SBF

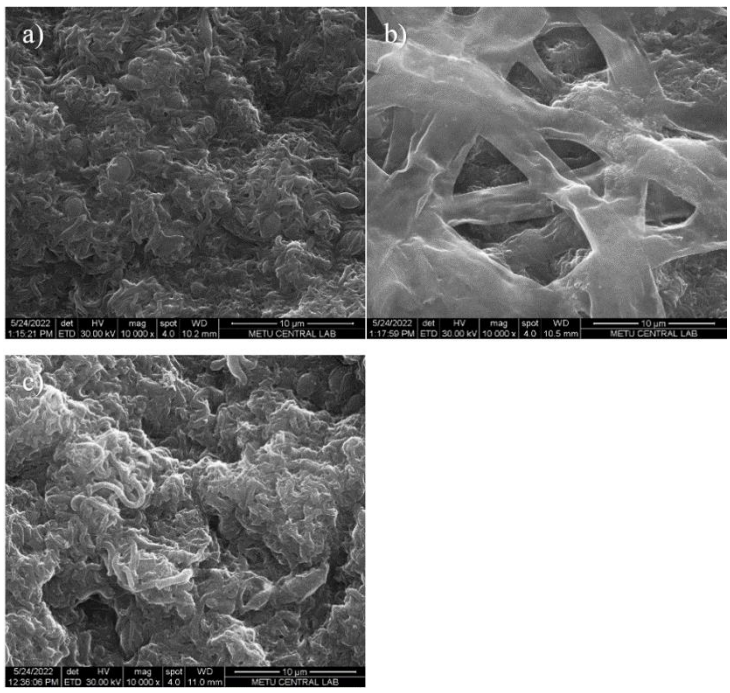

Figure 30. SEM images of 2.5% FHA incorporated sPEEK scaffolds: a) after 1 day in SBF b) after 7 days in SBF c) after 14 days in SBF

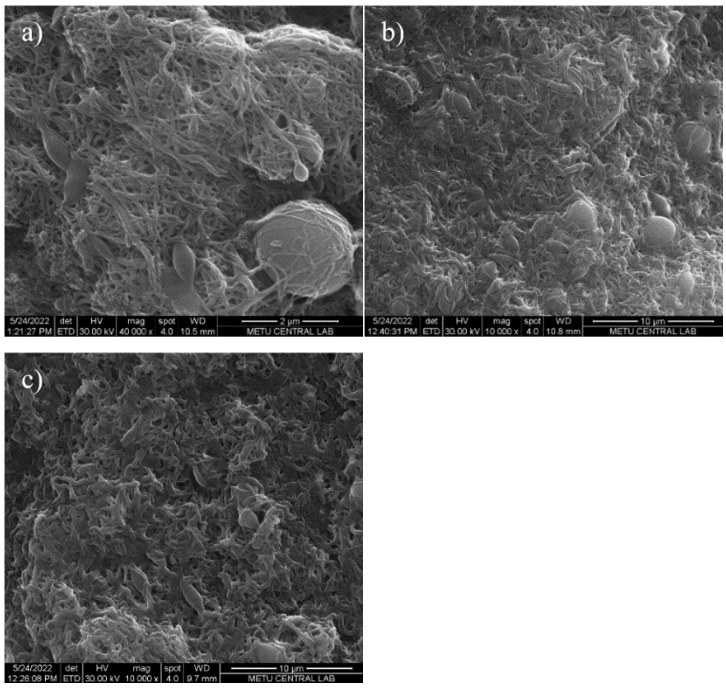

Figure 31. SEM images of 5% FHA incorporated sPEEK scaffolds: a) after 1 day in SBF b) after 7 days in SBF c) after 14 days in SBF

3.4 Cell Viability

Saos-2 cells proliferation on each scaffold (n=4) was determined with Alamar blue activity test for 1, 4 and 7 days. At the first day HA and FHA loaded groups showed significantly better results in comparison to the bare sPEEK scaffold. 1% FHA was significantly better than %2.5 and 5% FHA and other groups at the 4th day. On the fourth day general trend was growth but due to higher standard deviations in some groups changes were statistically insignificant. On the seventh day SPEEK group showed growth, 1%HA and 5%HA showed significantly high growth while 1%FHA showed decrease and other groups' changes were insignificant despite having a growth trend. All groups developed as such that they reached a similar point at the end of the experiment. This may indicate that the scaffolds reached a maximum of cell baring capacity.

In summary it can be said that scaffolds don't appear to have cytotoxic effect on Saos-2 cells. In the beginning 1%FHA group showed significant effect in accelerating the

proliferation of cells in comparison to other groups but at the seventh day cell viability of all scaffolds were comparable.

SEM Results of cell seeded scaffold at 7 day showed that for only sPEEK group there was a thin layer of cells covering the scaffold surface, but for all bioceramic groups the cell layer on surface was very thick (dense) and suggesting higher biocompatibility and proliferative capacity for these composite groups.

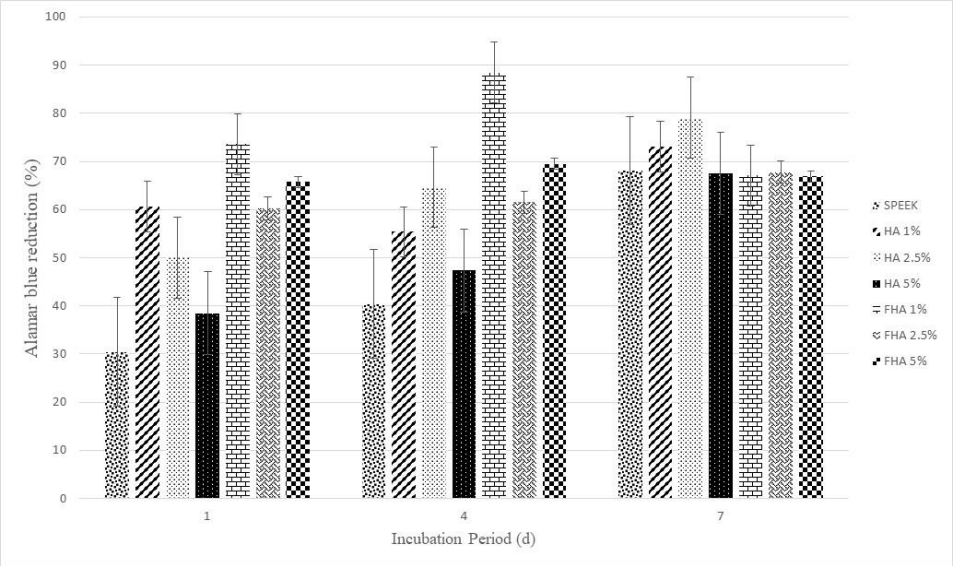

Figure 32. Cell viability of scaffolds by Alamar blue reduction test in day 1, 4, and 7

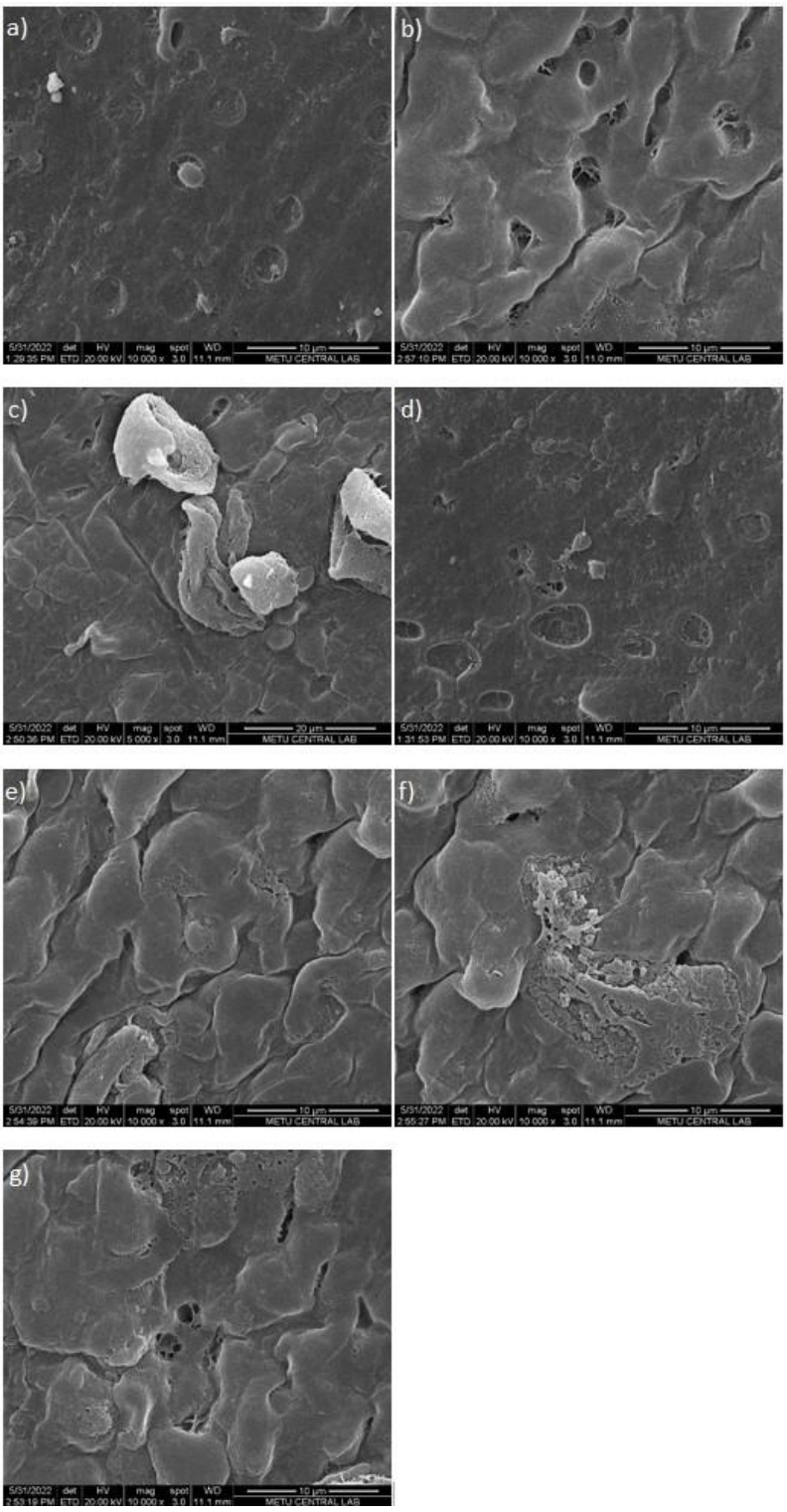

Figure 33. SEM images of scaffolds after 7 days of seeding Saos-2 cells: a) sPEEK b) 1% HA incorporated sPEEK scaffolds c) 2.5% HA incorporated sPEEK scaffolds d) 5% HA incorporated sPEEK scaffolds e) 1% FHA incorporated sPEEK scaffolds f) 2.5% FHA incorporated sPEEK scaffolds g) 5% FHA incorporated sPEEK scaffolds

CHAPTER 4

Conclusion

Due to various reasons, need for medical interventions for bone tissue is rising in number and the traditional methods of grafting are not able to answer the need. Synthetic bone scaffolds are a way to answer the demand in a safe and optimum way. This study aimed to investigate sulfonated polyether ether ketone electrospun scaffolds incorporated with different rations of HA and FHA as a potential biomaterial for Bone tissue engineering purpose. HA and FHA synthesis were verified with characterization tests. It was found that sPEEK had degradation profile in PBS indicating its improved hydrophilicity. Addition of either HA or FHA improved biomineralization of the scaffolds considerably. With FHA mineralization was recognized even at earlier time points than HA. In vitro experiments with Saos-2 cells show that FHA in optimum ratios is less cytotoxic than HA and incorporation of both HA and FHA in optimum ratios into the sPEEK scaffolds enhance cell proliferation. Among groups, considering all properties 1% FHA*sPEEK can be suggested as the most promising one.

RFERENCES

Alam, F., Varadarajan, K. M., Koo, J. H., Wardle, B. L., & Kumar, S. (2020). Additively Manufactured Polyetheretherketone (PEEK) with Carbon Nanostructure Reinforcement for Biomedical Structural Applications. *Advanced Engineering Materials*, *22*(10), 2000483. https://doi.org/10.1002/ADEM.202000483

Amini, A. R., Laurencin, C. T., & Nukavarapu, S. P. (2012a). Bone Tissue Engineering: Recent Advances and Challenges. *Critical Reviews in Biomedical Engineering*, *40*(5), 363. https://doi.org/10.1615/CRITREVBIOMEDENG.V40.I5.10

Amini, A. R., Laurencin, C. T., & Nukavarapu, S. P. (2012b). Bone Tissue Engineering: Recent Advances and Challenges. *Critical Reviews in Biomedical Engineering*, *40*(5), 363. https://doi.org/10.1615/CRITREVBIOMEDENG.V40.I5.10

an Investigation of Microstructure , Microhardness and Biocompatibility Characteristics of Yttrium Hydroxyapatite Doped With Fluoride a Thesis Submitted To the Graduate School of Natural and Applied Sciences of Middle East Technical University By Sidika M. (2010). *January*.

B, C. (2008). Normal bone anatomy and physiology. *Clinical Journal of the American Society of Nephrology : CJASN*, *3 Suppl 3*(Suppl 3). https://doi.org/10.2215/CJN.04151206

Bhardwaj, N., & Kundu, S. C. (2010). Electrospinning: A fascinating fiber fabrication technique. *Biotechnology Advances*, *28*(3), 325–347. https://doi.org/10.1016/J.BIOTECHADV.2010.01.004

bone - Chemical composition and physical properties | Britannica. (n.d.). Retrieved April 19, 2022, from https://www.britannica.com/science/bone-anatomy/Chemical-composition-and-physical-properties

Bone Structure – Anatomy & Physiology. (n.d.). Retrieved May 10, 2022, from

http://pressbooks-dev.oer.hawaii.edu/anatomyandphysiology/chapter/bone-structure/

Boyce, B., Yao, Z., & Xing, L. (2009). Osteoclasts have Multiple Roles in Bone in Addition to Bone Resorption. *Critical Reviews in Eukaryotic Gene Expression*, *19*(3), 171. https://doi.org/10.1615/CritRevEukarGeneExpr.v19.i3.10

Brum, R. S., Monich, P. R., Berti, F., Fredel, M. C., Porto, L. M., Benfatti, C. A. M., & Souza, J. C. M. (2019). On the sulphonated PEEK for implant dentistry: Biological and physicochemical assessment. *Materials Chemistry and Physics*, *223*, 542–547. https://doi.org/10.1016/J.MATCHEMPHYS.2018.11.027

Cartilage, Bone & Ossification: The Histology Guide. (n.d.). Retrieved May 9, 2022, from https://www.histology.leeds.ac.uk/bone/bone_types.php

Characterization of a Human Osteosarcoma Cell Line (Saos-2) with Osteoblastic Properties | Cancer Research | American Association for Cancer Research. (n.d.). Retrieved June 27, 2022, from https://aacrjournals.org/cancerres/article/47/18/4961/491558/Characterization-of-a-Human-Osteosarcoma-Cell-Line

Clarke, B. (2008). Normal Bone Anatomy and Physiology. *Clinical Journal of the American Society of Nephrology : CJASN*, *3*(Suppl 3), S131. https://doi.org/10.2215/CJN.04151206

Cooke, D. W., Divall, S. A., & Radovick, S. (2016). Normal and Aberrant Growth in Children. *Williams Textbook of Endocrinology*, 964–1073. https://doi.org/10.1016/B978-0-323-29738-7.00024-1

Delaisse, J.-M. (2014). The reversal phase of the bone-remodeling cycle: cellular prerequisites for coupling resorption and formation. *BoneKEy Reports*, *3*. https://doi.org/10.1038/BONEKEY.2014.56

Dong, Y., Liu, X., Song, T., & He, S. (2021). Topology optimization for structure with multi-gradient materials. *Structural and Multidisciplinary Optimization*, *63*(3), 1151–1167. https://doi.org/10.1007/S00158-020-02749-3

Dridi, A., Riahi, K. Z., & Somrani, S. (2021). Mechanism of apatite formation on a

poorly crystallized calcium phosphate in a simulated body fluid (SBF) at 37 °C. *Journal of Physics and Chemistry of Solids*, *156*, 110122. https://doi.org/10.1016/J.JPCS.2021.110122

Ghassemi, T., Shahroodi, A., Ebrahimzadeh, M. H., Mousavian, A., Movaffagh, J., & Moradi, A. (2018). Current Concepts in Scaffolding for Bone Tissue Engineering. *Archives of Bone and Joint Surgery*, *6*(2), 90. https://doi.org/10.22038/abjs.2018.26340.1713

Gong, C., Zheng, X., Liu, H., Wang, G., Cheng, F., Zheng, G., Wen, S., Law, W. C., Tsui, C. P., & Tang, C. Y. (2016). A new strategy for designing high-performance sulfonated poly(ether ether ketone) polymer electrolyte membranes using inorganic proton conductor-functionalized carbon nanotubes. *Journal of Power Sources*, *325*, 453–464. https://doi.org/10.1016/J.JPOWSOUR.2016.06.061

Haider, A., Haider, S., & Kang, I. K. (2018). A comprehensive review summarizing the effect of electrospinning parameters and potential applications of nanofibers in biomedical and biotechnology. *Arabian Journal of Chemistry*, *11*(8), 1165–1188. https://doi.org/10.1016/J.ARABJC.2015.11.015

He, Q., Xiao, X., Wang, W., Huang, Y., He, J., & Xiao, K. (2017). A novel gas conductor–gas barrier (GC–GB) blending membrane with adjustable gas separation capacity. *RSC Advances*, *7*(85), 53907–53915. https://doi.org/10.1039/C7RA09953C

Huang, R. Y. M., Shao, P., Burns, C. M., & Feng, X. (2001). Sulfonation of poly(ether ether ketone)(PEEK): Kinetic study and characterization. *Journal of Applied Polymer Science*, *82*(11), 2651–2660. https://doi.org/10.1002/app.2118

Jaber, H. L., & Kovács, T. A. (2019). Preparation and synthesis of hydroxyapatite bio-ceramic from bovine bone by thermal heat treatment. *Epitoanyag - Journal of Silicate Based and Composite Materials*, *71*(3), 98–101. https://doi.org/10.14382/epitoanyag-jsbcm.2019.18

JADE® Pattern Converter. (n.d.).

Kim, I. Y., Sugino, A., Kikuta, K., Ohtsuki, C., & Cho, S. B. (2009). Bioactive composites consisting of PEEK and calcium silicate powders. *Journal of Biomaterials Applications*, *24*(2), 105–118. https://doi.org/10.1177/0885328208094557

Kokubo, T., Kushitani, H., Sakka, S., Kitsugi, T., & Yamamuro, T. (1990). Solutions able to reproduce in vivo surface-structure changes in bioactive glass-ceramic A-W3. *Journal of Biomedical Materials Research*, *24*(6), 721–734. https://doi.org/10.1002/JBM.820240607

Koons, G. L., Diba, M., & Mikos, A. G. (2020). Materials design for bone-tissue engineering. *Nature Reviews Materials 2020 5:8*, *5*(8), 584–603. https://doi.org/10.1038/s41578-020-0204-2

Kulanthaivel, S., Mishra, U., Agarwal, T., Giri, S., Pal, K., Pramanik, K., & Banerjee, I. (2015). Improving the osteogenic and angiogenic properties of synthetic hydroxyapatite by dual doping of bivalent cobalt and magnesium ion. *Ceramics International*, *41*(9), 11323–11333. https://doi.org/10.1016/J.CERAMINT.2015.05.090

Liu, X., Smith, L. A., Hu, J., & Ma, P. X. (2009). Biomimetic nanofibrous gelatin/apatite composite scaffolds for bone tissue engineering. *Biomaterials*, *30*(12), 2252–2258. https://doi.org/10.1016/j.biomaterials.2008.12.068

Liu, Y., He, J. H., Yu, J. Y., & Zeng, H. M. (2008). Controlling numbers and sizes of beads in electrospun nanofibers. *Polymer International*, *57*(4), 632–636. https://doi.org/10.1002/PI.2387

McGee-Lawrence, M. E., Secreto, F. J., & Syed, F. A. (2013). Animal Models of Bone Disease-B. *Animal Models for the Study of Human Disease*, 391–417. https://doi.org/10.1016/B978-0-12-415894-8.00017-8

Measuring cytotoxicity or proliferation - alamarBlue Assay Protocol | Bio-Rad. (n.d.). Retrieved May 7, 2022, from https://www.bio-rad-antibodies.com/measuring-cytotoxicity-proliferation-spectrophotometry-fluorescence-alamarblue.html

Mohamed, A. M. F. S. (2008). An Overview of Bone Cells and their Regulating Factors of Differentiation. *The Malaysian Journal of Medical Sciences : MJMS*, *15*(1), 4. /pmc/articles/PMC3341892/

Mohsenpour, S., Kamgar, A., & Esmaeilzadeh, F. (2018). Investigation the Effect of TiO2 Nanoparticles on Proton Exchange Membrane of sPEEK Used as a Fuel Cell Electrolyte Based on Phase Diagram. *Journal of Inorganic and Organometallic Polymers and Materials*, *28*(1), 63–72. https://doi.org/10.1007/S10904-017-0723-5/FIGURES/8

Molecular cloning: a laboratory manual. (n.d.). Retrieved June 23, 2022, from https://www.cabdirect.org/cabdirect/abstract/19901616061

Nasker, P., Samanta, A., Rudra, S., Sinha, A., Mukhopadhyay, A. K., & Das, M. (2019). Effect of fluorine substitution on sintering behaviour, mechanical and bioactivity of hydroxyapatite. *Journal of the Mechanical Behavior of Biomedical Materials*, *95*, 136–142. https://doi.org/10.1016/J.JMBBM.2019.03.032

Nokoorani, Y. D., Shamloo, A., Bahadoran, M., & Moravvej, H. (2021). Fabrication and characterization of scaffolds containing different amounts of allantoin for skin tissue engineering. *Scientific Reports 2021 11:1*, *11*(1), 1–20. https://doi.org/10.1038/s41598-021-95763-4

Pimentel, C. A., de Lima Souza, J. W., dos Santos, F. S. F., de Sá, M. D., Ferreira, V. P., de Carvalho Barreto, G. B., Rodrigues, J. F. B., de Sousa, W. J. B., Filho, C. O. B., de Sousa, F. K. A., & Fook, M. V. L. (2019). Sulfonated poly(ether ether ketone)/hydroxyapatite membrane as biomaterials: process evaluation. *Polímeros*, *29*(1). https://doi.org/10.1590/0104-1428.01018

Polyetheretherketone (PEEK) - Polyetherether Ketone (PEEK) - Matmatch. (n.d.). Retrieved May 14, 2022, from https://matmatch.com/materials/mbas042-general-polyetheretherketone-peek-

Raggatt, L. J., & Partridge, N. C. (2010). Cellular and Molecular Mechanisms of Bone Remodeling. *The Journal of Biological Chemistry*, *285*(33), 25103. https://doi.org/10.1074/JBC.R109.041087

Rahmati, M., Mills, D. K., Urbanska, A. M., Saeb, M. R., Venugopal, J. R., Ramakrishna, S., & Mozafari, M. (2021). Electrospinning for tissue engineering applications. *Progress in Materials Science*, *117*, 100721. https://doi.org/10.1016/J.PMATSCI.2020.100721

Rutkovskiy, A., Stensløkken, K.-O., & Vaage, I. J. (2016). Osteoblast Differentiation at a Glance. *Medical Science Monitor Basic Research*, *22*, 95. https://doi.org/10.12659/MSMBR.901142

Schaffler, M. B., & Kennedy, O. D. (2012). Osteocyte Signaling in Bone. *Current Osteoporosis Reports*, *10*(2), 118. https://doi.org/10.1007/S11914-012-0105-4

Sefat, F., Mozafari, M., & Atala, A. (2019). Introduction to tissue engineering scaffolds. *Handbook of Tissue Engineering Scaffolds: Volume One*, 3–22. https://doi.org/10.1016/B978-0-08-102563-5.00001-0

Sun, X. Y., Chen, J. Y., Rao, C. Y., & Ouyang, J. M. (2020). Size-Dependent Cytotoxicity of Hydroxyapatite Crystals on Renal Epithelial Cells . *International Journal of Nanomedicine*, *15*, 5043–5060. https://doi.org/10.2147/IJN.S232926

Tariverdian, T., Sefat, F., Gelinsky, M., & Mozafari, M. (2019). Scaffold for bone tissue engineering. *Handbook of Tissue Engineering Scaffolds: Volume One*, 189–209. https://doi.org/10.1016/B978-0-08-102563-5.00010-1

Tereshchenko, V. P., Kirilova, I. A., Sadovoy, M. A., & Larionov, P. M. (2015). The materials used in bone tissue engineering. *AIP Conference Proceedings*, *1688*. https://doi.org/10.1063/1.4936017

Truesdell, S. L., Saunders, M. M., Truesdell, S. L., & Saunders, M. M. (2020). Bone remodeling platforms: Understanding the need for multicellular lab-on-a-chip systems and predictive agent-based models. *Mathematical Biosciences and Engineering 2020 2:1233*, *17*(2), 1233–1252. https://doi.org/10.3934/MBE.2020063

Vaezi, M., & Yang, S. (2015). Extrusion-based additive manufacturing of PEEK for biomedical applications. *Virtual and Physical Prototyping*, *10*(3), 123–135.

https://doi.org/10.1080/17452759.2015.1097053

Vallet-Regí, M., & Navarrete, D. A. (2015). CHAPTER 1 Biological Apatites in Bone and Teeth. *RSC Nanoscience and Nanotechnology*, *2016-January*(39), 1–29. https://doi.org/10.1039/9781782622550-00001

Van Gaalen, S., Kruyt, M., Meijer, G., Mistry, A., Mikos, A., Beucken, J. van den, Jansen, J., De Groot, K., Cancedda, R., Olivo, C., Yaszemski, M., & Dhert, W. (2008). Tissue Engineering of Bone. *Tissue Engineering*, 559–610. https://doi.org/10.1016/B978-0-12-370869-4.00019-7

Verbruggen, S. W. (2013). Mechanobiological Origins of Osteoporosis. *National University of Ireland, Galway*, *September 2013*, 7–10. https://doi.org/10.13140/RG.2.2.20595.32802

Wang, W., Luo, C. J., Huang, J., & Edirisinghe, M. (2019). PEEK surface modification by fast ambient-temperature sulfonation for bone implant applications. *Journal of the Royal Society, Interface*, *16*(152), 20180955–20180955. https://doi.org/10.1098/RSIF.2018.0955

Wong, K. L., Wong, C. T., Liu, W. C., Pan, H. B., Fong, M. K., Lam, W. M., Cheung, W. L., Tang, W. M., Chiu, K. Y., Luk, K. D. K., & Lu, W. W. (2009). Mechanical properties and in vitro response of strontium-containing hydroxyapatite/polyetheretherketone composites. *Biomaterials*, *30*(23–24), 3810–3817. https://doi.org/10.1016/j.biomaterials.2009.04.016

Xin, T., Gu, Y., Cheng, R., Tang, J., Sun, Z., Cui, W., & Chen, L. (2017). Inorganic Strengthened Hydrogel Membrane as Regenerative Periosteum. *ACS Applied Materials and Interfaces*, *9*(47), 41168–41180. https://doi.org/10.1021/ACSAMI.7B13167/SUPPL_FILE/AM7B13167_SI_001.PDF

Yang, X., Chen, X., & Wang, H. (2009). Acceleration of osteogenic differentiation of preosteoblastic cells by chitosan containing nanofibrous scaffolds. *Biomacromolecules*, *10*(10), 2772–2778. https://doi.org/10.1021/bm900623j

Yuan, Y., Liu, C., Qian, J., Wang, J., & Zhang, Y. (2010). Size-mediated

cytotoxicity and apoptosis of hydroxyapatite nanoparticles in human hepatoma HepG2 cells. *Biomaterials*, *31*(4), 730–740. https://doi.org/10.1016/J.BIOMATERIALS.2009.09.088

Zaidi, S. M. J., Mikhailenko, S. D., Robertson, G. P., Guiver, M. D., & Kaliaguine, S. (2000). Proton conducting composite membranes from polyether ether ketone and heteropolyacids for fuel cell applications. *Journal of Membrane Science*, *173*(1), 17–34. https://doi.org/10.1016/S0376-7388(00)00345-8

Zhang, Y., & Rehmmann, L. (2022). Extraction of high-value compounds from marine biomass via ionic liquid-based techniques. *Innovative and Emerging Technologies in the Bio-Marine Food Sector*, 417–439. https://doi.org/10.1016/B978-0-12-820096-4.00002-X

Zhao, F., Hu, S., Wang, F., & Wang, L. (2019). A sulfonated PEEK/PCL composite nanofibrous membrane for periosteum tissue engineering application. *Journal of Materials Science*, *54*(18), 12012–12023. https://doi.org/10.1007/s10853-019-03728-w